Findings of the Joint Dark Energy Mission Figure of Merit Science Working Group

Andreas Albrecht, Luca Amendola, Gary Bernstein, Douglas Clowe, Daniel Eisenstein, Luigi Guzzo, Christopher Hirata, Dragan Huterer, Robert Kirshner, Edward Kolb, Robert Nichol

(Dated: Dec 7, 2008)

These are the findings of the Joint Dark Energy Mission (JDEM) Figure of Merit (FoM) Science Working Group (SWG), the FoMSWG. JDEM is a space mission planned by NASA and the DOE for launch in the 2016 time frame. The primary mission is to explore the nature of dark energy. In planning such a mission, it is necessary to have some idea of knowledge of dark energy in 2016, and a way to quantify the performance of the mission. In this paper we discuss these issues.

I. THE UNKNOWN NATURE OF DARK ENERGY

The discovery that the universe is expanding with an ever-increasing velocity is now a decade old, yet there is no compelling theoretical explanation. We have a cosmological standard model, called ΛCDM, that seems capable of accounting for (at least in principle) all cosmological observations, including the apparent acceleration. But it is sobering to note that in ΛCDM as much as 95% of the present mass-energy of the universe is not understood, with only 5% of the present mass-energy in the form of "stuff" we understand (baryons, radiation, neutrinos). The rest of the present mass-energy of the universe is assumed to be dark: about 30% in the form of dark matter providing the bulk of the gravitational binding energy of galaxies, galaxy clusters, and other large-scale structure, and about 70% in the form of dark energy driving the present expansion of the universe. Both dark matter and dark energy point to physics beyond the standard models of gravity or particle physics.

This paper is concerned with dark energy [1], the *primum mobile* for the present accelerated expansion of the universe.

While ΛCDM seems capable of accounting for all observations, the aim of cosmology is not simply to find a model that describes the observations, but rather to find one that agrees with observations *and* is also grounded in physical reality.[1] The most important task ahead is to discover the nature of the dark universe, in particular, dark energy.

To date, all indications of dark energy come from measuring the time evolution of the expansion history of the universe. In the standard Friedmann-Lemaître-Robertson-Walker (FLRW) cosmology, the expansion rate as a function of the scale factor a is given by the Friedmann equation[2]

$$H^2(a) = H_0^2 \left[\Omega_R a^{-4} + \Omega_M a^{-3} + \Omega_k a^{-2} + \Omega_{DE} \exp\left\{ 3 \int_a^1 \frac{da'}{a'} \left[1 + w(a') \right] \right\} \right]. \quad (1)$$

In this expression Ω_i is the present fraction of the critical density, $\rho_C = 3H_0^2/8\pi G$, in the form of component i; e.g., radiation (R), matter (M), curvature (k) and dark energy (DE). The parameter H_0 is the present value of the expansion rate of the universe (Hubble's constant). Finally, $w(a)$ is the ratio of the pressure to the energy density for dark energy, $w(a) = p(a)/\rho(a)$. If dark energy is Einstein's cosmological constant, $w(a) = -1$.

In framing the question of the nature of dark energy, it is useful to start with something that doesn't work: It is clear from the observations that the Einstein–de Sitter cosmological model (a spatially flat, matter-dominated, FLRW model) does not describe the recent expansion history of the universe. In FLRW models the Friedmann equation follows directly from the $0-0$ component of the Einstein equations, so the fact that the Einstein–de Sitter model fails can be expressed as

$$G_{00}(\text{spatially flat FLRW}) \neq 8\pi G T_{00}(\text{matter}). \quad (2)$$

There are two generally orthogonal directions in explaining the observations. The first direction is to assume there is, in addition to matter and radiation, a new type of "negative pressure" component to the energy density of the universe that would be added to the right-hand-side of Eq. (2). The other direction is modify the left-hand side of

[1] Cosmological models that describe observations but are not grounded in physical reality have been found in the past, but have been rejected in favor of models based on the laws of nature (see, e.g., [2]).

[2] The scale factor a is normalized to unity at present. It is related to the redshift z by $1 + z = 1/a$.

Einstein's equation by saying that either the metric used is inappropriate, or to interpret the failure of Eq. (2) as an indication that Einstein did not have the final word on gravity, and that there is effectively a modification of the left-hand-side of his equations.

A. Primary Dark Energy (the Right-Hand-Side of Einstein's equations)

Even before the observation of cosmic acceleration, physicists were familiar with two possible sources of cosmic acceleration. These two types of acceleration were already well established, to the point that they were discussed in basic textbooks. And both can be thought of as a new fluid that contributes to the stress tensor. In one case the density of the new fluid is constant (equivalent to Einstein's "cosmological constant"), and in the other the fluid density is dynamical ("quintessence").

If cosmic acceleration is driven by a new fluid, the first question is to discriminate between these two ideas by determining whether the fluid density is constant or dynamical.

1. Einstein's Cosmological Constant

The cosmological constant arises as an additional constant term in Einstein's equations. A FLRW universe with a cosmological constant with value Λ is equivalent to adding a matter component with density $\rho_\Lambda \equiv \Lambda/8\pi G$ and with equation of state $p = -\rho$ (or $w(a) = -1$). This equation of state describes a ρ_Λ that is constant throughout the evolution of the universe. Until the mid 1990's, a commonly held belief among particle physicists and cosmologists was that Λ was identically zero. For many, this belief was partly motivated by the fact that naïve calculations give quantum field contributions to Λ of order 10^{60} or 10^{120} times larger than observationally acceptable. Other possible contributions to the vacuum energy, like scalar field condensates, are also truly enormous compared to the allowed value. It was widely believed that finding some symmetry or dynamical process that sets Λ (including contributions from quantum fields) precisely to zero was the best hope to resolve this apparent discrepancy.

The observation of cosmic acceleration has forced radical changes to this thinking. Many theorists now favor a "string theory landscape" [3–5] where all possible values of Λ are represented in a "multiverse." Cosmology and particle physics truly become one in this picture, since what we see as our "fundamental" particles and forces would be dictated by our cosmological evolution around the landscape. Alternatively a single "pure" cosmological constant might be what nature has chosen, but that would lead to dramatic changes to how we think about cosmology, entropy, and "heat death" in our universe [6, 7].

A precision experiment supporting $w = -1$ would lend weight to these radical ideas, while any evidence for $w \neq -1$ would falsify most of them instantly.

2. Quintessence Models

Another widely held belief that has had growing support over the last few decades is that the universe underwent a period of *cosmic inflation* in the distant past. A period of cosmic inflation appears to explain many features observed in the universe today, some of which seemed puzzling before the idea of inflation.

Today, inflation is quite well understood in terms of its phenomenology, but it still has a number of unresolved foundational questions. Despite these, it is clear that cosmic inflation requires a period of cosmic acceleration that *cannot* be described by a cosmological constant. Cosmic inflation is understood to be driven by some matter field, typically called the "inflaton," which exhibits an equation of state $p = w\rho$. During inflation, w takes values that approach $w = -1$. Inflation is fundamentally a dynamical process: Not only must the universe enter and exit inflation (leading to large variations in w) but small deviations from $w = -1$ are also necessary throughout the inflationary period in order for the mechanisms of inflation to work properly.[3] Thus, to the extent one believes in cosmic inflation, one believes the universe has already realized in the distant past cosmic acceleration using a *dynamical* fluid.

Most dynamical theories of dark energy re-use many of the "rolling scalar field" ideas from inflation and go under the name "quintessence" [1]. Unfortunately, basic questions about how a quintessence field with the right sorts

[3] One probe of inflation is the search for gravitational waves produced during the inflationary epoch (for example through their impact on CMB polarization or directly using gravitational wave detectors). For common types of inflation such observations are equivalent to probing the deviations from $w(a) = -1$ during the inflationary epoch.

of couplings fits in a fundamental theory are in no better shape than our understanding of the inflaton. Still, the prominence of cosmic inflation in our understanding of modern cosmology, our long history of preferring $\Lambda = 0$ (see for example [8]) and the presence of several quintessence models with interesting motivations have generated considerable interest in applying these dynamical ideas to the acceleration. Furthermore, recent work has shown that results from advanced experiments could potentially rule out many or perhaps even most quintessence models entirely [9].

B. Modification of General Relativity (the Left-Hand Side of Einstein's Equations)

The Hubble diagram of Type Ia Supernovae implies the existence of dark energy only if we assume that the standard cosmological framework in which we interpret the observations is correct. Part of this basis is Einstein's General Theory of Relativity (GR), our current standard theory of gravity. In fact, instead of adding an extra term (dark energy) to the stress-energy tensor on the right side of Einstein's equations, one can devise modifications of the left side that reproduce the observations equally well. Attempts in this direction include higher-order curvature terms (as in so-called $f(R)$ theories, [10]), or higher-dimensional theories, as in *braneworld* models [11]. Clearly, this alternative explanation would have consequences as profound and revolutionary as the existence of dark energy. Either dark energy or modified gravity would point to physics beyond our standard models of particle physics and/or gravity.

Therefore, we feel that while the accurate characterization of the expansion history of the universe, $H(z)$, (which translates into an effective dark energy equation of state $w(z)$) is crucial for future experiments, it cannot be considered as the final word. The "acceleration problem" reduces to this simple quest for one function only if GR is the correct theory of gravity (and if the dark energy is very simple, for example a scalar field, i.e., quintessence). In general, methods providing independent measurements of distance and redshift probe the expansion history $H(z)$ (thus $w(z)$), but cannot tell whether this comes from a true extra fluid in the cosmic budget, or by a more elusive change in the laws of gravity.

Luckily, there may be an alternative way to tackle this problem. In addition to governing the overall expansion of the homogeneous universe, gravity is also responsible for the gradual build-up of the large-scale structure of the universe we observe. The efficiency of this mechanism at different epochs, i.e., the "growth rate" of density fluctuations $f(z)$, depends not only on how fast the universe expands (thus on $H(z)$), but also on the very nature of the gravitational force. Measurements of $f(z)$ (or its integral, the "growth factor" $G(z)$) can break the above degeneracy between simple dark energy models and modified gravity.

The growth factor can be obtained from different observables. When matter density fluctuations have low amplitude, in the so-called linear regime of growth, their evolution on sub-horizon scales is easy to describe through a second-order differential equation, $\ddot{\delta} + 2H\dot{\delta} = 4\pi \mathrm{G}\rho\delta$. Here δ is the relative density excess with respect to the mean density of matter ρ. The source term on the right side of this equation depends directly on the theory of gravity: the form used here is correct only if GR is correct (and if one makes the very reasonable assumption that primary dark energy, if it exists, is not clustered on these scales). This equation has a growing solution such that we can write it as the product of a spatial part $D(\vec{x})$ and a time-dependent part $G(a)$ [where time is here parametrized via the cosmic scale factor $a(t)$, related to the redshift by $1 + z = 1/a(t)$]. Again, $G(a)$ is the growth factor and its derivative $f(a) = d\ln(G)/d\ln(a)$ is the growth rate. Given a measured $H(a)$ (which appears on the left-hand-side of the $\ddot{\delta}$ equation) and a theory of gravity (that determines the right-hand-side), the resulting $G(a)$ is uniquely predicted. A discrepancy in this prediction with a direct measurement of $G(a)$ would be a strong hint that GR breaks down on very large scales.

Measurements of galaxy clustering at different epochs provide information on $G(a)$, once the *bias* function mapping mass fluctuations into galaxy fluctuations is known. The bias issue can be overcome by *weak lensing tomography*, which probes directly the amplitude of mass fluctuations in redshift slices. Galaxy peculiar velocities depend directly on the derivative of $G(a)$, i.e., on $f(a)$, and can be measured from *redshift-space distortions* in large redshift surveys of galaxies. The growth factor $G(a)$ also enters in determining the number density and evolution of *rich clusters of galaxies* expected above a given mass threshold at a given redshift.

In fact, the fully relativistic treatment of the growth of small scalar perturbations shows that they have to be described in terms of two functions, ϕ and ψ, which are a generalization of the Newtonian gravitational potential. In standard Einstein's gravity with an ordinary dark sector the *anisotropic stress*, defined as $\phi - \psi$, vanishes. Galaxy clustering and peculiar velocities depend only on ψ, since neither strong fields nor high velocities are involved in the process. The dual nature of the potential can be evidenced only under relativistic conditions. This is the case for *gravitational lensing*, a phenomenon that is not present in the classical theory of Newton and which is sensitive to both potentials. As such, it is virtually the only experimental technique capable of detecting a non-zero anisotropic stress, i.e., a distinction between the two potentials (another probe is provided by the Integrated Sachs-Wolfe effect on the CMB, but with much lower sensitivity). Such a finding would be a strong indication of either modified gravity

or new physics in the dark sector.

As this is a Working Group for a space-based JDEM, we will not discuss other searches for departures from GR. We only note here that precision GR tests, e.g., solar system tests, already severely restrict the possible departures from GR, although constraints obtained on local scales do not necessarily apply to cosmological scales.

The implications of this simple reasoning is that the problem of cosmic acceleration depends on measuring (a) the expansion history; (b) the growth history, and (c) the two gravitational potentials.

C. Further Alternatives

A third possibility is to postulate that the formation of structure at late times leads to large deviations from the isotropic and homogeneous FLRW metric. Toy models have been constructed (most of them using a Lemaître-Tolman-Bondi (LTB) metric). These can explain the data without dark energy, although at the price of introducing large and so-far unobserved inhomogeneities. These toy models can be tested, e.g., by combining an angular diameter distance (like tangential BAOs) with a direct measurement of the expansion rate $H(z)$ (e.g., from radial BAOs).

D. The Task Before Us

The standard cosmological model assumes that dark energy is described by a cosmological constant. While this is the simplest possibility, the magnitude of Λ is difficult to understand, and, of course, we seek tests of this hypothesis.

Thus, when discussing ways to probe dark energy, we will adopt the approach of the Dark Energy Task Force (DETF) [12] and assume that the observational program should be to

1. determine as well as possible whether the accelerating expansion is consistent with a cosmological constant, i.e., unevolving dark-energy density,
2. measure as well as possible any time evolution of the dark energy density, and
3. search for a possible failure of general relativity through comparison of the effect of dark energy on cosmic expansion with the effect of dark energy on the growth of cosmological structures.

In this report we establish a framework for assessing progress toward those goals. Section II reviews the Fisher-matrix methodology by which the power of experiments is described; Section III describes the FoMSWG cosmological model and its free parameters. Section IV describes the knowledge of these parameters that we expect at the advent of the JDEM era, with details of these pre-JDEM "data models" given in the Appendices. The FoMSWG finds that potential payload implementations and observational strategies should be judged on their advancement over this set of standardized pre-JDEM data models. Section V describes quantities and plots which we suggest be used to gauge the effectiveness of proposed JDEM investigations, and which can be derived from the Fisher matrices of JDEM data models. Section VI presents guidelines for the interpretation of our suggested plots and figures of merit.

We do not discuss the important issue of systematic errors in dark energy measurements, nor do we discuss the optimization of a dark energy program to accomplish the three goals above. Again, it is important to stress that our goal is simply to establish a framework for assessing progress.

II. THE FISHER INFORMATION MATRIX

The FoMSWG adopted a strategy of describing the potential of any given dark energy investigation by its Fisher information matrix over the parameters of a standardized cosmological model. In this section, we review the meaning of the Fisher matrix and typical manipulations required to implement the FoMSWG evaluations of experimental scenarios. In the following section we describe the cosmological model adopted by the FoMSWG.

The Fisher matrix method was used by the Dark Energy Task Force and is standard in many fields. It is instructive to consider first a simple case: suppose we observe a series of quantities y_b, $b \in \{1, \ldots B\}$, each of which has Gaussian uncertainties σ_b. Suppose in addition that each observable should be described by a function f_b of some parameters p. The common χ^2 value is (we will assume y_b for different b are uncorrelated)

$$\chi^2 = \sum_{b=1}^{B} \frac{(f_b(p) - y_b)^2}{\sigma_b^2}. \tag{3}$$

If the parameters p describe the true universe, then the likelihood of a given set of observations is

$$P(y) \propto \exp\left(-\frac{1}{2}\chi^2\right). \tag{4}$$

The problem, however, is to estimate parameters p given a realization of the data y. Using Bayes' theorem with uniform prior, we have $P(p|y) \propto P(y|p)$, so that the likelihood of a parameter estimate can be described as a Gaussian with the same χ^2, now viewed as a function of parameters. If we expand about the true values of the parameters, $p^i = p^i_0 + \delta p^i$, and average over realizations of the data,

$$\left\langle \chi^2(p) \right\rangle = \left\langle \chi^2 \right\rangle + \left\langle \frac{\partial \chi^2}{\partial p^j} \right\rangle \delta p^j + \frac{1}{2} \left\langle \frac{\partial^2 \chi^2}{\partial p^j \partial p^k} \right\rangle \delta p^j \delta p^k + \dots \tag{5}$$

where the expectation values are taken at the true values p_0. The mean value of observable y_b is indeed $f_b(p_0)$, so the second term vanishes. The distribution of errors in the measured parameters is thus in the limit of high statistics proportional to

$$\exp\left(-\frac{1}{2}\chi^2\right) \propto \exp\left(-\frac{1}{4}\left\langle \frac{\partial^2 \chi^2}{\partial p^j \partial p^k} \right\rangle \delta p^j \delta p^k\right) = \exp\left(-\frac{1}{2}\mathcal{F}_{jk}\delta p^j \delta p^k\right) \tag{6}$$

where the Fisher matrix is

$$\mathcal{F}_{jk} = \sum_b \frac{1}{\sigma_b^2} \frac{\partial f_b}{\partial p^j} \frac{\partial f_b}{\partial p^k}. \tag{7}$$

From this expression it follows that

$$\left\langle \delta p^j \delta p^k \right\rangle = \left(\mathcal{F}^{-1}\right)^{jk}, \tag{8}$$

In other words, the covariance matrix is simply the inverse of the Fisher matrix (and vice versa).

More generally, if one can create a probability $P(p^i|y_b)$ of the model parameters given a set of observed data, e.g., by Bayesian methods, then one can define the Fisher matrix components via

$$\mathcal{F}_{ij} = -\left\langle \frac{\partial^2 \ln P}{\partial p^i \partial p^j} \right\rangle \tag{9}$$

and the Cramer-Rao theorem states that any unbiased estimator for the parameters will deliver a covariance matrix on the parameters that is no better than $\mathcal{F}^{-1}$. The Fisher matrix therefore offers a best-case scenario for one's ability to constrain cosmological parameters given a set of observations.

The Fisher matrix is useful for planning a suite of experiments, because the constraints using the ensemble of experiments are described by the *sum* of the Fisher matrices of each component experiment. This is clear from $\mathcal{F} \propto \ln P$. Prior information can also be included the same way. Furthermore, there are other straightforward manipulations of the Fisher matrix that yield the expected constraints on subsets or reparametrizations of the original parameter set. We offer details on these procedures below.

A. Fisher Matrix Manipulations

There has been some concern about degenerate or ill-conditioned Fisher matrices, for instance the Planck prior given by DETF. In practice, such (near) degeneracies are an accurate reflection of the inability to distinguish all the cosmological parameters in a particular experiment's data. We need, however, to be careful that round off error in Fisher-matrix calculations does not significantly change the constraints implied by the matrix.

One strategy to avoid ill-conditioned matrices is to keep all the parameter variations at the same order of magnitude. This is one motivation for putting all distances into c/H_{100} units and for using logarithmic quantities for parameters.

A second strategy is to be careful about inverting Fisher matrices, doing so only when necessary and properly handling the potentially large covariances that result.

We now discuss manipulations of Fisher matrices and discuss proper handling where appropriate.

1. Priors

A Gaussian prior with width σ can be placed on the i^{th} parameter by adding to the appropriate diagonal element of the Fisher matrix:

$$\mathcal{F}_{kl} \longrightarrow \mathcal{F}_{kl} + \frac{\delta_{ki}\delta_{li}}{\sigma^2} \qquad \text{(no sum on } i\text{)}, \tag{10}$$

which can also be written as

$$\mathcal{F} \longrightarrow \mathcal{F} + \mathcal{F}^p, \tag{11}$$

where in this case $\mathcal{F}^p$ is an extremely simple matrix with a single non-zero diagonal element $1/\sigma^2$ in the i^{th} row and column.

If the prior on p_i is intended to be very strong, the addition of a large $1/\sigma_i^2$ to $\mathcal{F}$ can cause numerical instabilities in some algorithms for inversion of the matrix. An infinitely strong prior on p_i is equivalent to simply striking the ith row and column from the Fisher matrix.

2. Projection onto new variables

A common operation is to transform the Fisher matrix in some variable set p^i into a constraint on a new variable set q^i. The formula for this is to generate the derivative matrix $\mathcal{M}$ with $\mathcal{M}^i{}_j = \partial p^i/\partial q^j$. In the simple case of Gaussian errors on observables, the new Fisher matrix is

$$\mathcal{F}'_{lm} = \sum_b \frac{1}{\sigma_b^2}\frac{\partial f_b}{\partial q^l}\frac{\partial f_b}{\partial q^m} = \sum_b \frac{1}{\sigma_b^2}\frac{\partial p^j}{\partial q^l}\frac{\partial p^k}{\partial q^m}\frac{\partial f_b}{\partial p^j}\frac{\partial f_b}{\partial p^k} = \frac{\partial p^j}{\partial q^l}\frac{\partial p^k}{\partial q^m}\mathcal{F}_{jk} = (\mathcal{M})^T\,\mathcal{F}\,\mathcal{M} \tag{12}$$

using the usual summation convention on j, k. The result holds when we generalize to arbitrary likelihood functions.

No numerical instabilities are generated by having $\mathcal{F}$ or $\mathcal{M}$ be rank-deficient, so remapping onto a new variable set will not generally raise numerical issues. A small eigenvalue for $\mathcal{F}'$ will simply indicate a poorly constrained direction in the $\vec{q}$ space for this experiment. For example if $\vec{q}$ is of higher dimension than $\vec{p}$, then the constraint on $\vec{q}$ must be degenerate at the Fisher-matrix level of approximation.

If one wants to add a prior on some quantity that is not a single parameter of the Fisher matrix, one can work in variables where it is a single parameter and then transform the diagonal $\widehat{\mathcal{F}}^p$ (where the hat indicates that the new variables are used) back into the working variables using the inverse of the transformation given in Eq. (12). In general, if the prior can be expressed as a likelihood over the parameter set, it can be assigned a Fisher matrix via Eq. (9).

B. Marginalization

On many occasions we need to produce a Fisher matrix in a smaller parameter space by marginalizing over the uninteresting "nuisance" parameters. This amounts to integrating over the nuisance parameters without assuming any additional priors on their values.

Suppose the full parameter vector set is $\vec{p}$, which is a union of two parameter sets: $\vec{p} = \vec{q} \cup \vec{r}$, and we are really only interested in the Fisher matrix for the parameter set $\vec{q}$. The Fisher matrix $\mathcal{F}'$ for parameters $\vec{q}$ after marginalization over $\vec{r}$ can be expressed as

$$\mathcal{F}' = \mathcal{F}_{qq} - \mathcal{F}_{qr}\mathcal{F}_{rr}^{-1}\mathcal{F}_{rq}. \tag{13}$$

Here $\mathcal{F}_{rr}$, etc., are submatrices of $\mathcal{F}$.

A common, but numerically unstable procedure, is to

1. invert $\mathcal{F}$,
2. remove the rows and columns, corresponding to $\vec{r}$, that are being marginalized over,
3. then invert the result to obtained the reduced Fisher matrix.

This will fail for an ill-conditioned $\mathcal{F}$. Using Eq. (13) is more stable, since degeneracies in $\mathcal{F}_{qq}$ are properly propagated to $\mathcal{F}'$ with no instability. One need worry only about an ill-conditioned $\mathcal{F}_{rr}$ submatrix, i.e., the experiment has a poor constraint on some of the marginalized parameters. One should check for this by diagonalizing $\mathcal{F}_{rr} = U\Lambda U^T$, where $\Lambda = \mathrm{diag}(\lambda_1, \lambda_2, \ldots)$ and U is orthogonal. Now

$$\mathcal{F}' = \mathcal{F}_{qq} - (\mathcal{F}_{qr}U)\,\Lambda^{-1}\,(\mathcal{F}_{qr}U)^T\,. \tag{14}$$

If one finds that λ_i is small, then one needs to examine row i of $\mathcal{F}_{qr}U$: if it is (near) zero, then this degeneracy in r does not propagate into parameters q upon marginalization, and it is safe to ignore this eigenvector. In other words: if there is some component to r that is uncorrelated with q, we do not care whether r was constrained by the experiment.

The remaining case where roundoff is a potential problem is when Λ has a small eigenvalue that does not have a correspondingly small row in $\mathcal{F}_{qr}U$. This means that there was a component of $\vec{q}$ that was highly covariant with a component of $\vec{r}$, such that marginalization over r can leave the q component poorly constrained. Roundoff error might lead to $\mathcal{F}'$ indicating a weak constraint on q^i when there should be none. But our exposure to this kind of problem should be very small, since the fallacious constraints induced by roundoff error will be weak.

When we are combining the constraints from experiments A and B, we will be summing their Fisher matrices. In general any marginalization over nuisance parameters must be done *after* summation of the two Fisher matrices. If, however, the nuisance parameters of A are disjoint from those of B, then the two data sets have independent probability distributions over the set of nuisance parameters, and it is permissible to marginalize before summation.

III. THE FIDUCIAL COSMOLOGICAL MODEL

We have to choose a fiducial cosmological model. We choose the standard Friedmann-Lemaître-Robertson-Walker cosmology. Our fiducial cosmological model also assumes that $w(a) = -1$. The other parameters of the fiducial cosmological model relevant for dark energy data models are (note that the numbering begins at 0 and not 1).

0. n_S, the primordial scalar perturbation spectral index.
1. ω_M, the present value of $\Omega_M h^2$, where Ω_M is the ratio of the present value of the ratio of the total (baryons plus dark matter) mass density, ρ_M, to the critical density, $\rho_C = 3H_0^2/8\pi G$, and h is the reduced Hubble constant, $H_0 = 100h$ km s^{-1}Mpc^{-1}.
2. ω_B, the present value of $\Omega_B h^2$, where Ω_B is the ratio of the present value of the ratio of the baryon mass density to the critical density.
3. ω_k, the present value of $\Omega_k h^2$, where Ω_k is the ratio of the present value of the ratio of the effective curvature mass density to the critical density. From the Friedmann equation, $\Omega_k = 1 - \Omega_M - \Omega_{DE} - \Omega_R$, where Ω_R is the contribution of radiation.
4. ω_{DE}, the present value of $\Omega_{DE} h^2$, where Ω_{DE} is the ratio of the present value of the ratio of the dark energy density to the critical density.
5. $\Delta\gamma$, the change in the growth factor from the standard GR result. So the actual growth factor is $f_{\rm actual}(z) = f_{\rm GR}(z)[1 + \Delta\gamma \ln \Omega_M(z)]$. This forces $f(z) \to 1$ at high redshift.
6. $\Delta\mathcal{M}$, the difference between the absolute magnitude of a type Ia supernova and its fiducial value.
7. G_0, the normalization of the linear growth function in the era when JDEM has sensitivity to growth, taken to be $z < 9$. It is given relative to the GR predication of growth between the recombination era and $z = 9$: $G_{\rm actual}(z = 9) = G_0 \times G_{\rm GR}(z = 9)$. It is assumed that any decaying mode excited during the Dark Ages is gone by this time (i.e., before we can plausibly observe it). The fiducial value is $G_0 = 1$.
8. $\ln \Delta^2_\zeta(k_\star)$, where ζ is the primordial curvature perturbation and k_* is the pivot scale, here chosen to be 0.05 Mpc^{-1} (note: *not* $0.05\,h$ Mpc^{-1}).

Some comments are in order.

1. We also need to state the definition of the nonlinear power spectrum with $\Delta\gamma$ turned on. Since this is not a fundamental parameter but a phenomenological one there are many possible definitions. We are using the definition that at a particular redshift, the $\Delta\gamma$ parameter does *not* change the mapping from the linear-to-nonlinear $P(k)$ (the NL $P(k)$ only changes through implicit dependence of linear $P(k)$ on $\Delta\gamma$). This prevents an experiment from measuring the full $P(k)$ at one redshift and claiming a constraint on $\Delta\gamma$; one has to measure the evolution in $P(k)$ or have velocities in order to do this.

2. It is not necessary to specify the fiducial value of $\mathcal{M}$.

3. We need not specify H_0, since $\omega_M + \omega_{DE} + \omega_k = h^2$, so H_0 is a derived value.

We take the values of the parameters of the fiducial cosmology to be the ΛCDM model of WMAP5:

$$\begin{aligned} n_S &= 0.963 \\ \omega_M &= 0.1326 \\ \omega_B &= 0.0227 \\ \omega_k &= 0 \\ \omega_{DE} &= 0.3844 \\ \Delta\gamma &= 0 \\ \Delta\mathcal{M} &= 0 \\ \ln G_0 &= 0 \\ \ln \Delta^2_\zeta(k_\star) &= -19.9628 \quad . \end{aligned}$$

Using $\omega_M + \omega_{DE} + \omega_k = h^2$, the derived value of h is 0.719, which implies a Hubble constant of $H_0 = 71.9$ km s^{-1}Mpc^{-1}. Our choices also imply $\sigma_8 = 0.798$.

A. Modeling the dark-energy equation of state parameter w

While the DETF model for $w(a)$ was very simple: $w(a) = w_0 + (1-a)w_a$, here we wish to consider a more general behavior. We will model $w(a)$ as piecewise constant values of $w(a)$ defined in bins of $\Delta a = 0.025$ starting at $a = 0.1$ so that there are 36 bins total. So we will define w_i, $i = 0, \ldots, 35$ to be a number describing the value of w in the interval between $a = 1 - 0.025i$ and $a = 1 - 0.025(i+1)$ or equivalently between $z = 0.025i/(1-0.025i)$ and $z = 0.025(i+1)/[1-0.025(i+1)]$.

In the fiducial model, $w_i = -1$ for $i = 0, \ldots 35$.

B. Format of the Fisher Matrix

Here we establish the ordering and format of the Fisher matrix. Since Fisher matrices for different techniques will be combined, the format for every Fisher matrix must be identical.

When we specify the values of the Fisher matrix, we use the ordering

0	n_S
1	ω_M
2	ω_B
3	ω_k
4	ω_{DE}
5	$\Delta\gamma$
6	$\Delta\mathcal{M}$
7	$\ln G_0$
8	$\ln \Delta_\zeta(k_*)$
9	w_0
10	w_1

$$\begin{array}{ll} \vdots & \vdots \\ 44 & w_{35} \end{array}$$

Note that the ordering begins with 0, not 1, and for $0 \leq i \leq 35$, entry $9+i$ corresponds to w_i.

We denote by $\mathcal{F}_{ij}$ the ij component of the Fisher matrix. The Fisher matrix is symmetric. By convention, unless specified, it is assumed that $\mathcal{F}_{ij} = 0$. The Fisher matrix is supplied in ascii format in the form

$$i \quad j \quad \mathcal{F}_{ij}. \tag{15}$$

A line that begins with a "#" is considered to be a comment line.

It is necessary to specify the Fisher matrix in double precision.

IV. DARK ENERGY CIRCA 2016

Here we will not go into detail about how the pre-JDEM[4] Fisher matrices are constructed, rather, we relegate that to an appendix. However, we would like to make the important point that although considerable effort went into constructing the Fisher matrices, they should be used with caution, since any data model purporting to represent the state of knowledge eight years in the future is highly suspect.

We note that our assumed improvements in SN measurements for pre-JDEM are conservative, in the sense no significant advances in techniques or astrophysical knowledge are assumed before JDEM.

For our WL Fisher matrix, we assumed some improvements in the systematic error budgets as detailed in the Appendix. This is reasonable as there are identifiable (though not necessarily guaranteed) paths toward improving these errors. We have also been conservative in not assuming the use of all WL information (e.g., we do not include the bispectrum, and included only one of the WL surveys) or any theoretical knowledge about intrinsic alignments. Overall we believe the WL Fisher matrix is somewhat conservative but not extremely conservative.

We have been more optimistic about the expected advances in our knowledge for the BAO technique, e.g., measuring the BAO scale at high redshift using Lyman-alpha galaxies or absorbers, and the reconstruction method of Eisenstein et al. [13]. We feel this is justified as the strength of the BAO method is that the distance between optimism and pessimism is smaller (see the DETF report).

A. Prospective Additional Probes of Dark Energy

1. Galaxy Clusters (Number Density, Clustering and Their Evolution)

The abundance and clustering of galaxy clusters is another promising technique, and has previously been considered by the DETF [12]. There are many means of identifying and measuring galaxy clusters; the main source of uncertainty in future applications of this method will be in determining the relation of the selection function and observables to the underlying mass of the clusters. In this report we chose not to include clusters in our pre-JDEM Fisher matrix, because we were unable to forecast its level of systematic error in mass determination ca. 2016 with any useful degree of reliability. Since all methods are challenged by sources of systematic errors, some common among them and some independent, there is value in addressing dark energy with all feasible techniques, including cluster studies. Here, we briefly review the potential of the cluster technique.

Clusters are a very promising technique, in particular because X-ray, Sunyaev-Zeldovich (SZ) and optical and near-infrared (NIR) data can be combined to minimize systematic errors in identifying and characterizing the cluster population. Present cluster data and systematic errors determine cosmological parameters, particularly σ_8, to accuracy similar to present weak-lensing data.

Mass selection systematics are smallest for X-ray- or SZ-selection [14], and there is concrete hope for further reduction in these uncertainties in the near future. Within the halo model framework, key elements for cluster cosmology are the form of the observable signal likelihood as a function of mass and redshift, and the effects of projection (including non-cluster sources) on measured signals. X-ray-selected surveys have particular advantage in

[4] In this section we discuss projections of knowledge of dark energy parameters in the "pre-JDEM" time frame. To be explict, by pre-JDEM projects we mean projects that we expect will have a cosmological likelihood function available before JDEM is begins its first data analysis.

the latter aspect; although AGN emission is a contaminant that can only be removed with sufficiently high-resolution X-ray data. All signals require empirical calibration of low-order moments, particularly variance, in the scaling relations. X-ray [15, 16] and SZ [17, 18] signals have local calibrations with statistical and systematic errors in slope and intercept at the level of about 10%, with considerable potential to improve with higher quality data.

Compared to X-ray or SZ methods, optical- and NIR-selected cluster surveys are more strongly affected by blending of multiple halos in projection, a long-standing problem known to Abell. Multi-color information provides the photometric redshift information that can significantly reduce projection effects. Estimates for single-color photometric selection indicate that low-mass leakage (i.e., smaller halos that, viewed in alignment, appear as a single, rich system) adds a 10 to 20% enhancement in number relative to the traditional mass selection [19].

Optical samples offer the benefit of extending the cluster population to lower masses than is achievable by X-ray and SZ. This could potentially decrease the shot noise by factors of several if confusion due to projection can be accurately modeled in the low richness regime. Theoretical elements needed to achieve successful modeling of projection effects are: 1) the halo mass function, 2) halo clustering bias, and 3) multi-color galaxy occupation models that describe both central and satellite galaxies in halos out to redshifts $z \sim 1.5$. The form of this last element, which is only now being studied, is a crucial source of systematic uncertainty that must be overcome in order for optical richness to function as a viable mass proxy.

The situation will improve significantly when deep samples dramatically increase the current sparse numbers of high clusters, allowing "self-calibration" of scaling relations [20, 21]. In imagining future developments, one should keep in mind that all current measurements of cosmological parameters with clusters are based on samples of only a few hundred objects [14, 22–24]. In light of this, one should be optimistic given the set of funded projects that will return data in the next decade: 1) South Pole Telescope (SPT) and Atacama Cosmology Telescope (ACT) will reveal many thousands of new SZ clusters above about $2 \times 10^{14} M_{\odot}$ over several thousand sq deg; 2) Dark Energy Survey (DES) and UK VISTA will overlap the SPT area with optical/NIR for photo-z estimates and additional mass calibration, and 3) a new X-ray survey mission, e-Rosita, will launch in 2012 and cover $20,000$ sq. deg. to a flux limit nearly two orders of magnitude fainter than the present ROSAT All-Sky Survey. Combining homogeneous X-ray, SZ and optical/NIR samples across large areas of sky will provide unprecedented sensitivity to distant clusters. Such data, extended with targeted, multi-wavelength follow-up by ground- and space-based observatories, will provide critical cross-calibration abilities that will serve to mitigate sources of systematic error associated with cluster selection and signal–mass characterization.

Galaxy clusters can also be detected and measured using weak gravitational lensing shear. Since lensing shear responds directly to mass, systematic errors in mass assignment are bypassed. This has been exploited to determine the mean mass of x-ray or optically selected clusters via "stacking" of lensing signals [25]. Future deep WL surveys could usefully detect clusters, or, more precisely, shear peaks. Any JDEM executing WL shear tomography would obtain the necessary data for this cosmological test. Such a technique removes the power spectrum from the shear tomography measurement, resulting in a purely geometric determination of angular distance ratios. While such a measurement will have a lower signal-to-noise ratio than the full WL survey, it would provide an internal check for any systematic errors in the survey.

2. Redshift-Space Distortions

Redshift-space distortions in the clustering pattern of galaxies have recently been the subject of renewed significant attention in the context of dark energy as a method to trace the evolution of the growth rate of structure with redshift [26]. The linear part of redshift distortions is induced by the coherent motions of galaxies partaking in the overall growth of overdensities. By measuring galaxy two-point correlations along and perpendicular to the line-of-sight, one can quantify the distortions in terms of the linear compression parameter β, which is related to the growth rate f as $f = b_L \times \beta$ [27] (in this expression b_L is the *linear bias* parameter of the class of galaxies being used as tracers of large-scale structure). This provides, in principle, a way to detect evidence for modified gravity as an alternative solution to the accelerated expansion problem. Conversely, if General Relativity is assumed, this technique provides one further method to constrain the evolution of the equation of state $w(a)$, through a precise measurement of $\Omega_M(z)$ at different redshifts[28, 29].

The practical application of redshift-space distortions as an acceleration probe is still in its infancy: spectroscopic samples beyond $z > 0.5$ are just now starting to be large enough as to allow extraction of the linear signal from the noise, overcoming at the same time cosmic variance. A positive aspect, however, is that due to the intense investigations performed during the 1990's on local samples (as e.g., the IRAS surveys), there exist significant technical knowledge on how to account and correct for systematic and nonlinear effects [30]. Monte Carlo forecasts based on mock surveys indicate that it is possible to reach statistical errors on β of the order of a few percent within surveys extending to $z \sim 1$ with densities of objects of order 10^{-2} to $10^{-3} h^3$ Mpc^{-3} and covering volumes about 10^8 to

$10^9 h^{-3}$ Mpc^3 [26]. A JDEM-class survey providing 100 million redshifts spread through 10 redshift bins between 0.5 and 2, would reach similar percent accuracy on β within each bin, constraining not only a simple "γ-model" for the growth rate, but also the detailed evolution of $f(z)$ itself [31]. This is for example the kind of survey planned by the European mission EUCLID.

In fact [32, 33], redshift-space distortions constrain the combination $\sigma_8(z) \times f(z)$, which in the assumption of linear deterministic bias, corresponds to the observed product $\beta \times \sigma_8$(galaxies). When combined with the high-redshift normalization of the power spectrum from CMB observations (e.g., Planck), this enables one to determine the product $G(z)f(z)$. An independent determination of the galaxy bias, e.g., from the bispectrum [34], would enable both $G(z)$ and $f(z)$ to be measured separately. Recent theoretical work [35, 36] suggests in addition that using two classes of galaxy tracers with different bias factors, should allow one to reach even higher accuracies. This awaits confirmation through mock surveys with realistic noise properties, however, it is a clear indication of the active developments in this area. While current constraints on the growth rate are at the several tens of percent level (e.g., [26, 32]), progress is rapid. It is reasonable, therefore, to predict redshift-space distortions to emerge in the next decade as one of the main tools of investigation for cosmic acceleration.

3. The Integrated Sachs-Wolfe (ISW) Effect

When a photon passes through a time-dependent gravitational potential, its energy changes. This effect produces a secondary (i.e., not primordial) anisotropy in the CMB [37] that is correlated with large scale structure [38]. This anisotropy is known as the integrated Sachs-Wolfe (ISW) effect. Since gravitational potentials vary with cosmic time according to $\Phi \propto G(a)/a$, a cross-correlation of the CMB with large-scale structure at a particular redshift z allows one to probe the rate of growth of cosmic structure at that redshift. The signal depends on the rate of change of gravitational potential $\dot{\Phi}$, which is proportional to $(f-1)G$. This is very attractive from a systematics point of view since $f \approx 1$ during most of the history of the universe:[5] Nature takes the difference $f-1$ for us, unlike redshift-space distortions (proportional to Gf) or weak lensing (where $G(z)$ is measured using source galaxies at different redshifts, and then differentiated to get f). Recent ISW analyses combining WMAP with low-redshift data have come close to their ideal statistical error limits [39, 40] and the technique has one of the highest levels of maturity. The largest systematic has been chance correlations of Galactic foregrounds on the largest angular scales with extragalactic structures; microwave emission from extragalactic objects (even AGNs) has turned out to be subdominant to the ISW effect at the angular scales of interest. With the broad frequency coverage of the upcoming Planck mission it is reasonable to expect that in the 2016 timeframe the ISW effect will be essentially statistics-limited outside the Galactic Plane region.

The downside to the ISW effect is that the ISW signal has exactly the same frequency dependence as the primordial CMB anisotropies, and hence the latter constitute an irreducible noise source. Indeed, it is expected that the latter will limit the ISW detection significance approximately to the $7.5 f_{\rm sky}^{1/2}$ σ level [41]. Constructing a Fisher matrix based on the signal and noise estimates of Afshordi [41] we find that even a "perfect" ISW program out to $z = 2$ covering 2/3 of the sky and reaching the sampling variance limit ($nP \gg 1$) makes little improvement to the dark energy constraints: for example, adding it to our pre-JDEM prior improves the DETF FoM from 116 to 120. It would have an effect on modified gravity constraints: $\sigma(\Delta\gamma)$ improves from 0.21 to 0.08. We emphasize that this is *not* included in the FoMSWG pre-JDEM standard prior, since not all of the relevant large-scale structure data will exist in 2016. We also note that ongoing studies of JDEM weak-lensing programs suggest that these can constrain $\Delta\gamma$ much more tightly than even the perfect ISW program. That said, the ISW effect will always be valuable as a cross-check, and as a test of more general modified gravity phenomenologies (e.g., scale-dependent $\Delta\gamma$). It may also provide a competitive constraint on $\Delta\gamma$ in the pre-JDEM era, depending on the level of systematics and nuisance parameter requirements encountered by other probes of the growth of structure.

4. The Alcock-Paczynski Effect

The anisotropic clustering of galaxies also contains a probe of the distance scale through the Alcock-Paczynski effect [42–45]. This provides a measurement of $H(z) \times D_A(z)$, which is important by itself but becomes particularly useful as a way to convert constraints on $D_A(z)$ from BAO or SNe into constraints on $H(z)$. However, this effect

[5] We have $f = 1$ in the matter-dominated era, assuming GR.

is mixed together with the dynamical redshift-space distortions and their interaction with galaxy bias. The relative weight of these two effects depends on the redshift and their signatures are in principle separable through detailed modeling. At $z \sim 1$ dynamical distortions dominate [26] and attempts to model both from galaxy data show strong degeneracy [46]. Similarly to the case of dynamical redshift distortions, improved theoretical modelling in the coming decade could change this situation and unlock a significant new test of dark energy from galaxy redshift surveys.

V. ON QUANTIFYING THE MERIT OF DARK-ENERGY MISSIONS

In this section we describe how to extract useful figure(s) of merit from the 45×45 Fisher matrix describing any suite of experiments, which succinctly summarize progress toward the goals described in Sec. I D.

Each Fisher matrix is of dimension 45×45, corresponding to nine cosmological parameters and 36 piecewise constant equation of state parameters w_i, $i \in \{0, 35\}$. If a method is insensitive to a given parameter p^k, then the corresponding Fisher elements $\mathcal{F}_{ik}$ will be zero for each i, but we still insist on retaining the full dimensionality of the matrix. Each technique t has a Fisher matrix $\mathcal{F}^t$. We can consider combinations of techniques by adding the corresponding Fisher matrices. The total efficacy can be found by summing the Fisher matrices for all techniques: $\mathcal{F}^{\rm total} = \sum_t \mathcal{F}^t$. We suggest that the procedures we outline herein should be performed using the Fisher matrix for each JDEM technique individually, as well as the techniques in combination.

A. Tests of smooth DE and ΛCDM

1. Principal components

In the principal component approach [47], we aim to understand the redshifts at which each experiment has the power to constrain w. One starts by expanding the equation of state as

$$1 + w(a) = \sum_{i=0}^{35} \alpha_i e_i(a), \tag{16}$$

where α_i are coefficients, and $e_i(a)$ are the eigenvectors to be defined below. The procedure for computing the principal components goes as follows:

1. Since in this section we are considering constraints on the equation of state, we fix the parameters $\Delta\gamma$ and G_0 to their fiducial values (0 and 1, respectively). This can be done by adding a strong prior to the corresponding diagonal elements of $\mathcal{F}$ ($\mathcal{F}_{55}$ and $\mathcal{F}_{77}$), as described in Sec. II A 1.

2. Now we wish to marginalize over all cosmological parameters except those corresponding to w_i. Section II B describes the matrix manipulations that implement marginalization.

3. Now rotate the parameters into a new basis by diagonalizing the marginalized Fisher matrix

$$\mathcal{G} = \mathcal{W}^T \mathbf{\Lambda} \mathcal{W}, \tag{17}$$

where $\mathbf{\Lambda}$ is diagonal and $\mathcal{W}$ is an orthogonal matrix. It is clear that the new parameters e_i, defined as $\mathbf{e} \equiv \mathcal{W}\mathbf{p}$, are uncorrelated, for they have the diagonal covariance matrix $\mathbf{\Lambda}^{-1}$. The e_i are referred to as the principal components and the rows of $\mathcal{W}$ are the window functions (or weights) that define how the principal components are related to the p_i. For a fixed i, the i^{th} row of $\mathcal{W}$ is the eigenvector $e_i(a_m)$, where a_m runs over the (discrete) values of the scale factor; $a_m \equiv 1 - (m + 1/2)\Delta a$ with $m \in \{0, 35\}$. Elements of the matrix $\mathbf{\Lambda}$ are the corresponding eigenvalues λ_i.

4. We normalize the amplitude of each eigenvector so that

$$\int e_i^2(a) da \to \sum_m e_i^2(a_m) \Delta a = 1, \tag{18}$$

(where, recall, $\Delta a = 0.025$ is the binning width in scale factor), and we correspondingly renormalize the eigenvalues λ_i as well. We can now compute the coefficients of the expansion of $1 + w(z)$ in Eq. (16) as

$$\alpha_i = \int [1 + w(a)] e_i(a) da \to \sum_m [1 + w(a_m)] e_i(a_m)\, \Delta a. \tag{19}$$

We do not explicitly use the coefficients α_i (note that their values are all trivially zero for a ΛCDM model anyway). We are however interested in the *variance* in these coefficients:

$$\sigma_i^2 \equiv \sigma^2(\alpha_i) = \frac{1}{\lambda_i}. \tag{20}$$

Finally, we rank-order the eigenvectors from best to worst measured, that is, by the value of σ_i^2 (smaller σ_i^2 have higher rank).

We choose the variance, σ_i^2, to be the appropriate measure rather than σ_i. Measurements that are limited by statistical errors have their variance improve inversely with the size of the data set. Hence, we focus on the ratio of variances as this can be interpretted as the ratio of the survey size, e.g., as measured by cost, effort, or time.[6]

A principal component is considered usefully constrained only if its variance σ_i^2 is less than unity, since in that case it limits the RMS fluctuation of the equation of state in that mode, $\langle[1+w(z)]^2\rangle = \sigma_i^2$, to be smaller than unity. In other words we have a prior prejudice that variations in w beyond $O(1)$ are unlikely. We impose this prior belief by performing the following operation

$$\frac{1}{\sigma_i^2} \to 1 + \frac{1}{\sigma_i^2} \quad \Rightarrow \quad \sigma_i^2 \to \frac{\sigma_i^2}{1+\sigma_i^2}, \tag{21}$$

This procedure regularizes the PC errors, i.e., sets $\sigma^2(\alpha_i)$ to be unity at worst, making the quantitative nature of the PC error plots (described below) easier to understand. For our pre-JDEM data, 15–20 of the best-determined PCs have raw variance $\sigma_i^2 < 1$, and approximately the first 10 of those are negligibly affected by the prior in Eq. (21). Since the JDEM principal components will be determined even better than the pre-JDEM ones, we see that our prior does not significantly affect the first 10–20 components, allowing the reader to infer the true intrinsic power of JDEM to probe $w(z)$.

The remaining step is to plot the principal components and the accuracies with which they are measured. We find that two plots are particularly useful:

1. A plot of the first three (or so) eigenvectors $e_i(z)$. We choose plotting them in redshift z rather than scale factor a since the former is more commonly used in observational cosmology. The best-measured eigenvectors most clearly indicate the redshifts at which the probe is capable of detecting variations in dark-energy density.

2. A plot of the eigenvector variance, σ_i^2 vs. i for the first 10 to 20 eigenvectors. It is most useful to quantify how much JDEM improves upon the pre-JDEM errors. This can be done by plotting the ratio

$$\frac{\sigma_i^{-2}(\text{JDEM})}{\sigma_i^{-2}(\text{pre-JDEM})}, \tag{22}$$

where pre-JDEM errors (that we project and provide in the appendix) approximate the accuracies available from combined ground-based surveys in year 2015. This ratio is generally greater than unity for any PC and, because of the regularization procedure in Eq. (21), the ratio will approach unity for poorly measured modes. The idea is to plot all accuracies that are measured better than unity, that is, up to the highest value of i for which $\sigma_i^2 \simeq 1$ (at which point the prior from Eq. (21) completely dominates $\sigma_i^2(\text{JDEM})$).

An example of a graph of the first principal components of a JDEM mission is shown in Fig. 1. In this example we see that technique A is sensitive to lower redshifts than the other techniques. The redshift sensitivity of the combined probes is dominated by techniques B and C in this particular example, because the two have very similar best-measured eigenvectors as the combination of the three.

Figure 2 shows the corresponding ratios $\sigma_i^{-2}(\text{JDEM})/\sigma_i^{-2}(\text{pre-JDEM})$. To construct this figure, it is necessary to know the values of $\sigma_i(\text{pre-JDEM})$. They are given in Table I.

---

[6] Of course, measurements that are limited by systematic errors or by parameter degeneracies broken only by external data sets will improve more slowly with size; it is not necessarily the case that one can improve the variance by a factor of 10 simply by running the experiment 10 times longer.

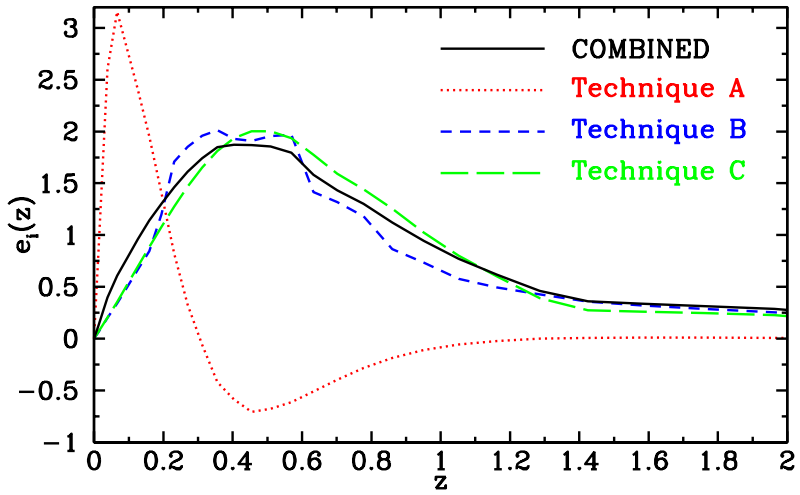

FIG. 1: An example of the first principal component for individual techniques, and all of the techniques combined.

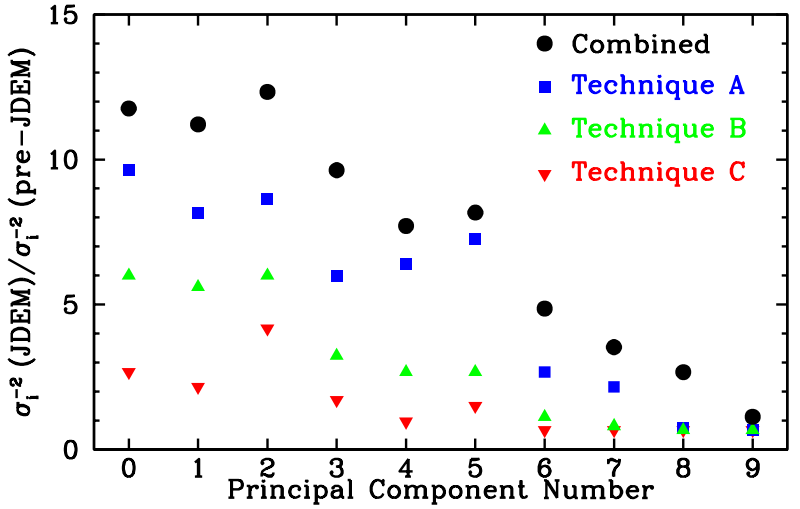

FIG. 2: An example of how one might present a graph of the increase in knowledge of the evolution of dark energy from a JDEM mission, normalized to the pre-JDEM knowledge. The data points shown in this figure do not correspond to any proposed JDEM, but invented merely to illustrate an example graph.

2. (w_0, w_a) and the pivot values

The DETF FoM remains a useful simple measure of an experiment's constraining power. Since the 36-parameter description of the equation of state is quite general, it is clear that we should be able to project straightforwardly the constraints on the w_i onto the parameters (w_0, w_a) used by the DETF. Projection of Fisher matrices onto new variables is discussed in Sec. II A 2. In this part of the analysis, one should *not* add priors to the principal components as in Eq. (21).

Let $\mathcal{H}$ be the desired 2×2 Fisher matrix in parameters w_0 and w_a. Then

$$\mathcal{H}_{ij} = \sum_{m,n} \frac{\partial w_m}{\partial p^i} \mathcal{G}_{mn} \frac{\partial w_n}{\partial p^j}, \tag{23}$$

i	σ_i(BAO)	σ_i(SN)	σ_i(WL)	σ_i(COMBINED)
1	0.027	0.103	0.061	0.021
2	0.058	0.211	0.134	0.044
3	0.090	0.381	0.231	0.069
4	0.116	0.567	0.337	0.094
5	0.158	0.768	0.493	0.121
6	0.190	0.883	0.628	0.158
7	0.250	0.956	0.657	0.188
8	0.289	0.984	0.783	0.239
9	0.348	0.993	0.851	0.276
10	0.396	0.998	0.922	0.324
11	0.418	0.999	0.943	0.386
12	0.456	1.000	0.980	0.390
13	0.533	1.000	0.996	0.451
14	0.581	1.000	0.998	0.521
15	0.620	1.000	0.999	0.534
16	0.662	1.000	0.999	0.595
17	0.734	1.000	1.000	0.668
18	0.768	1.000	1.000	0.726
19	0.801	1.000	1.000	0.764
20	0.851	1.000	1.000	0.795
21	0.900	1.000	1.000	0.824
22	0.926	1.000	1.000	0.862
23	0.945	1.000	1.000	0.905
24	0.961	1.000	1.000	0.929
25	0.970	1.000	1.000	0.955

TABLE I: Pre-JDEM values of σ_i for the first 25 best determined principal components for various techniques, plus the techniques combined.

where the parameters p are either w_0 or w_a. Moreover, the derivatives are trivially simple: $\partial w_m/\partial w_0 = 1$ and $\partial w_m/\partial w_a = 1 - a_m$; here a_m is the scale factor corresponding to the index m. Now that we have the matrix $\mathcal{H}$, the errors in w_0 and w_a are easy to obtain:

$$\sigma^2(w_0) = \left(\mathcal{H}^{-1}\right)_{w_0 w_0}, \tag{24}$$

$$\sigma^2(w_a) = \left(\mathcal{H}^{-1}\right)_{w_a w_a}. \tag{25}$$

Recall that the goal is to test whether or not dark energy arises from a cosmological constant ($w_0 = -1$, $w_a = 0$ in the DETF parametrization). For each data model the constraint on $w(a)$ varies with a. However, there is some pivot value of a, denoted by a_p, where the uncertainty in $w(a)$ in minimized for a given data model. The value of the scale factor (or redshift) with the minimun uncertainty is called the pivot scale factor (or redshift), a_p (or z_p). One can also define a pivot value of w as

$$w_p = w_0 + (1 - a_p) w_a. \tag{26}$$

Finally, we would also like to quote the pivot redshift z_p and the uncertainties in $w_p \equiv w(z_p)$. Since w_p is by definition uncorrelated with the parameter w_a, it is easy to show that

$$z_p = -\frac{\left(\mathcal{H}^{-1}\right)_{w_0 w_a}}{\left(\mathcal{H}^{-1}\right)_{w_0 w_a} + \left(\mathcal{H}^{-1}\right)_{w_a w_a}}, \tag{27}$$

$$\sigma^2(w_p) = \left(\mathcal{H}^{-1}\right)_{w_0 w_0} - \frac{\left[\left(\mathcal{H}^{-1}\right)_{w_0 w_a}\right]^2}{\left(\mathcal{H}^{-1}\right)_{w_a w_a}}. \tag{28}$$

The DETF FoM is $|\mathcal{H}|^{1/2} = 1/\sigma(w_p)\sigma(w_a)$.

B. Tests of general relativity through growth of structure

We also report accuracy in the "growth index" γ, defined in the fitting function for the linear growth of density perturbations:

$$G(a) = G_0 \exp\left(\int_{0.1}^{a} d\ln a\,[\Omega_M^{\gamma}(a) - 1]\right), \tag{29}$$

where $G(a) \equiv \delta/a$ is the growth of density perturbations normalized to Einstein-de Sitter case. The γ parametrization with $\gamma = 0.55$ was shown to closely approximate the exact solution within GR for a wide variety of physical dark energy equation of state ratios [48]; measuring a departure of γ from its fiducial value (0.55 in ΛCDM) therefore provides a test of general relativity. When computing γ, we allow the freedom in the parameter $\ln G_0$, and fully marginalize over all other parameters as well, including the equation of state parameters w_i.

We have found that the highest-redshift w_i bins are very poorly constrained by the data. These w_is can be partially degenerate with $\Delta\gamma$ because extremely large fluctuations in the dark energy at early times can re-excite the decaying mode of linear perturbations, thereby changing f and affecting the measurement of $\Delta\gamma$. Therefore, when marginalizing over the w_i (and only when marginalizing over the w_i), we add a prior of $\Delta a/100$ to the diagonal element of the Fisher matrix associated with each w_i. This prior is extremely weak–it corresponds to penalizing models where $|1+w|$ exceeds approximately 10–and it prevents numerical problems associated with the unconstrained w_is from leaking into $\sigma(\Delta\gamma)$.

VI. INTERPRETING THE FIGURES AND NUMBERS

Before presenting some broad guidelines for interpreting the information generated following the FoMSWG procedure outlined in the above section, it is important to stress that the FoMSWG feels that it would be ill advised to pursue a dark energy program on the sole basis of a figure of merit, or even several such numbers, or even the information generated following the FoMSWG procedure. Figures of merit, or the result of the FoMSWG procedure, are only as good as the data models used to generate them. Constructing a data model requires assumption about many things, in particular systematic errors and performance of instruments.

We feel it is important to emphasize several points:

1. We are operating under the assumption that the nominal launch date for JDEM will be sometime in 2016. Dark energy remains a compelling astrophysical question (perhaps the *most* compelling) and the creativity and imagination of astronomers and physicists will continue to be directed toward investigations into the nature of dark energy. Predictions of what will be known about dark energy, or what will be known about systematic uncertainties associated with dark energy measurements, eight years in the future are inherently unreliable. What we have reported about this subject is the informed judgment of the Working Group, but we must emphasize both the importance, and the inherent uncertainty, of such predictions.

2. We find that it is impossible to evaluate different dark energy investigations without the adoption of the same fiducial cosmological model and prior assumptions as a starting point. In this report we proposed a fiducial cosmological model and appropriate prior information to be used as a starting point.

3. Even with uniform fiducial cosmology and priors, 10–20% changes in these figures of merit can result from minor variation in assumptions about astrophysical parameters in each method, e.g., galaxy biases, SN rates, etc.

4. The FoMSWG finds that there is no single number that can describe the scientific reach of a JDEM. Our efforts have been directed toward producing a simple prescription that can be used to judge the potential scientific reach of a given dark energy investigation. While again, there is no single number, a few graphs and numbers can convey a lot of quantitative information. We have been prescriptive about this point.

5. Finally, although this is a Figure of Merit Working Group, we feel that it is important to emphasize that there are important criteria in the evaluation of an experimental framework or investigation that are not describable in terms of a figure of merit. For example, systematic errors will determine what an investigation will accomplish. Allowance for systematic errors should be part of the procedure used in generating each investigation's Fisher matrix. Important systematic errors are, however, sometimes difficult to quantify and sometimes even difficult to list.

With the above *caveat emptor*, we do feel that if one starts with reliable data models the information generated by following the FoMSWG procedure outlined in Sec. V can convey a lot of information. We now provide some guidance for interpretation of the various produces.

1. Graphs of Principal Components as a function of z: These graphs provide information about the redshift coverage and sensitivity of a particular technique or combinations of techniques. Because we have very little information about the behavior of dark energy with redshift, it is desirable to have wide redshift coverage. The sensitivity, on the other hand, is greatest at the redshift where the *strongest* principal components peak. The peak redshift and PC shapes are primarily determined by the cosmological technique (increasing from SN to BAO to WL), with a slightly weaker but important dependence on the survey specifications.

2. Graph of σ_i^{-2}(JDEM)/σ_i^{-2}(pre-JDEM): This graph is an indication of the advance of accuracy as the result of a JDEM. Recall that the DETF parametrized the evolution of dark energy by $w(a) = w_0 + w_a(1-a) = w_p + w_a(a_p - a)$. In this parametrization there were two parameters, which could be chosen to be either (w_0, w_a) or (w_a, w_p) (see Sec. V for a description). The DETF figure of merit was proportional to the inverse of the product of the uncertainties in these parameters: DETF FoM $\propto [\sigma(w_a) \times \sigma(w_p)]^{-1}$. Our corresponding parametrization is much more ambitious, and consists of 36 principal components of the function $w(a)$. We discussed in Sec. V a regularization procedure that imposes $\sigma_i^2 \to 1$ for large σ_i^2, so only usefully determined principal components will have large ratios of σ_i^{-2}(JDEM)/σ_i^{-2}(pre-JDEM). Existing computations of principal components show that improving an experiment tends to improve the measurement of all the independently measured modes in unison. Individuals may have different preferences whether to focus on the first few best-measured modes or a wider range of modes when assessing a given experiment. In either case, the graph of σ_i^{-2}(JDEM)/σ_i^{-2}(pre-JDEM) allows one to make an individual judgment and also note any interesting deviations from the "improvement in unison" result that may come up.

3. (w_0, w_a) and the pivot values (w_p, z_p): These numbers are trivially generated and provide a useful consistency check of the principal component analysis. For instance the pivot value z_p is the redshift where w is best determined. This pivot redshift is usually consistent with the redshift where the first principal component peaks. Furthermore, from w_0 and w_p once can construct the DETF figure of merit. One expects that the data models that result in better DETF figure of merits will result in larger values of σ_i^{-2}(JDEM)/σ_i^{-2}(pre-JDEM). Wild discrepancies would indicate the need to understand the reason.

4. $\sigma^{-2}(\Delta\gamma)$: This number indicates the ability of a program to test that the growth of structure follows that expected in GR. Larger values indicate greater power. Our data models for pre-JDEM results indicate a value of $\sigma(\Delta\gamma) = 0.21$. A JDEM should result in a smaller number. We note that $\sigma(\Delta\gamma)$ is primarily a test of GR at $z < 1$, as the FoMSWG cosmological model requires deviations from GR growth to be much larger at low z.

APPENDIX A: PREDICTIONS FOR THE PRE-JDEM FISHER MATRICES

1. Planck Fisher Matrix

CMB observations are valuable dark-energy studies because they (i) enable us to estimate the matter density ω_M and the distance $D_A(z = 1100)$ to the surface of last scattering; (ii) set the amplitude and shape of the matter power spectrum and length of the BAO standard ruler; and (iii) contain secondary anisotropies that carry low-redshift information such as the ISW effect, SZ effect, and lensing of the CMB. Accordingly, the FoMSWG constructed a Fisher matrix intended to model dark energy constraints from Planck. This Fisher matrix only contains the primary anisotropies; dark energy constraints from, e.g., the SZ effect would be considered part of the cluster technique. Its method of construction is similar to that of the DETF Planck matrix, but is not exactly the same.

The Fisher matrix was constructed using the Planck LFI 70 GHz and HFI 100 and 143 GHz channels using the "performance goal" beam and noise parameters from the Planck Blue Book [49]. Both temperature and E-mode polarization data were used over 70% of the sky. It was assumed that over this fraction of the sky the other channels could be used to remove foregrounds, and that the Planck beams could be mapped well enough that they would not be a limiting systematic.

In most cases, the Fisher matrix is constructed using the standard equation,

$$\mathcal{F}_{ij} = \frac{1}{2}\sum_{\ell=2}^{2000}(2\ell+1) f_{\rm sky} \mathrm{Tr}\left[(\mathbf{C}_\ell + \mathbf{N}_\ell)^{-1}\frac{\partial \mathbf{C}_\ell}{\partial p^i}(\mathbf{C}_\ell + \mathbf{N}_\ell)^{-1}\frac{\partial \mathbf{C}_\ell}{\partial p^j}\right], \tag{A1}$$

where i and j represent the cosmological parameters, ℓ is multipole number, $f_{\rm sky} = 0.7$ is the fraction of the sky observed, $\mathbf{C}_\ell$ is the 2×2 CMB power spectrum matrix (containing TT, TE, and EE spectra), and $\mathbf{N}_\ell$ is the 2×2 noise matrix.

The parameter space is the standard FoMSWG parameter space, augmented by the optical depth τ due to reionization. Two exceptions are made to the above rule.

1. For the cosmological parameters $X \in \{\Omega_{\rm K}, w_0 ... w_{35}\}$, we force the exact angular diameter distance by making the replacement:

$$\frac{\partial \mathbf{C}}{\partial X} \leftarrow \frac{\partial D_{\rm A}(z=1100)/\partial X}{\partial D_{\rm A}(z=1100)/\partial \omega_{\rm de}} \frac{\partial \mathbf{C}}{\partial \omega_{\rm de}}. \tag{A2}$$

   This exactly enforces the angular diameter distance degeneracy and removes any information from the power spectrum of the ISW effect.

2. The optical depth τ is unique in depending mainly on the lowest multipoles, even with Planck instead of WMAP. Observations have shown that these low CMB multipoles are below Galactic foregrounds in polarization over most of the sky at all frequencies [50], and reaching the Planck statistical uncertainty of $\sigma(\tau) \sim 0.005$ may be too optimistic. Moreover, the single-parameter step models of reionization are undoubtedly too simple and the ability to measure τ is degraded when one considers more generic possibilities. It is estimated that these uncertainties may limit Planck constraints on optical depth to about 0.01 [51]. We thus eliminated the $\ell < 30$ multipoles in the TE and EE spectra (i.e., we set $N_\ell^{EE} = \infty$) and replaced them with a prior on τ with $\sigma(\tau) = 0.01$. This prior dominates over any information about τ from the TT power spectrum.

We did not include primordial gravitational waves ("tensors") in the Fisher matrix. A Fisher matrix calculation shows that over $f_{\rm sky} = 0.7$, a tensor-to-scalar ratio of $r = 0.03$ is required to produce a 1σ change in the CMB TT power spectrum and $r = 0.06$ to produce a 2σ change.[7] On the timescale of JDEM, it is likely that B-mode observations will have reached or approached this level of precision. Moreover, tensors mainly affect the low multipoles ($\ell < 100$) whereas most of the Planck constraints relevant to dark energy come from higher multipoles (the exception, noted above, is τ). Thus at the level of accuracy of this report, it is reasonable to neglect tensors in dark energy forecasts even though they are well-motivated.

Since τ does not appear in any of the non-CMB cosmological probes, we marginalize it out of the Planck Fisher matrix before combining it with other information.

2. Pre-JDEM Weak Lensing Fisher Matrix

The FoMSWG projection of weak lensing data in ca. 2015 is based on estimates of the performance of the *Dark Energy Survey (DES)*, which has been recommended for CD-3b approval from the Department of Energy and plans to commence its survey around 2011 and to complete around 2016. A shallower, larger-area WL survey may be completed by this date by the *PanSTARRS* collaboration, but the available information was insufficient to evaluate its performance.

Our code is based on the DETF model, but with some improvements, most notably more thorough treatment of intrinsic alignments (described in detail in §A 2 b).

a. Survey parameters

For the DES we assume a sky coverage of 5000 deg^2, and a total effective source-galaxy density $n_{\rm eff} = 9\,{\rm arcmin}^{-2}$ with shape noise per galaxy of $\sigma_\gamma = 0.24$. We presume the sources to be distributed in redshift according to $dn_{\rm eff}/dz \propto z^2 e^{-z/z_0}$, with z_0 chosen to yield a median source redshift of 0.6. Photometric redshifts errors for DES are presumed to have a Gaussian distribution with $\sigma_z = 0.05(1+z)$. We ignore redshift outliers.

We divide the source population into 10 bins, sufficient to saturate the dark-energy information content. We consider information to be available from the 2-point correlations between all bin pairs. Each bin contains both galaxy-density and galaxy-shear observations. We include information from shear-shear correlations (i.e., cosmic

[7] Our normalization convention corresponds to $r = 16\epsilon$ in terms of the inflationary slow-roll parameter.

shear power spectrum) and shear-density correlations (the cross-correlation cosmography test). We have neglected non-Gaussian observables (3- and 4-point functions, WL peak or cluster counts, aperture mass PDFs, etc.) due to the difficulty of forecasting their systematic errors.

These codes consider all 2-point observables, plus systematic errors due to:

- shear calibration errors;
- photo-z biases;
- intrinsic alignments of galaxies (IA), both shape-shape correlations (II) and shape-density correlations (GI);
- weak prior constraints on the biases and correlation coefficients of galaxy density and intrinsic alignments with the mass distribution; and
- non-Gaussian covariance of convergence power spectra.

b. Formalism

Our code has not been described previously; there is substantial overlap with DETF but for purposes of reproducibility it is described here in detail.

We divide the source galaxies into $N_z = 10$ redshift slices (z-bins) and consider power spectra in each of $N_\ell = 18$ multipole bins (ℓ-bins). The z-bins have equal numbers of galaxies; their redshift centroids range from 0.18 (1st bin) to 1.41 (10th bin). The ℓ-bins are logarithmically spaced between $\ell = 12$ (1st bin) and $\ell = 7700$ (12th bin). In each angular bin we construct all power spectra and cross-spectra of the galaxy densities $\{g_i\}_{i=1}^{N_z}$ and convergences inferred from shear maps $\{\kappa_i\}_{i=1}^{N_z}$. There are $N_z(2N_z+1)$ such power spectra and cross spectra, and so we construct the length $N_\ell N_z(2N_z+1)$ vector of power spectra $\mathbf{C} = \{C^{\kappa\kappa}_{\ell ij}, C^{gg}_{\ell ij}, C^{g\kappa}_{\ell ij}\}$. A Fisher matrix requires (i) a model for $\mathbf{C}$ as a function of cosmological and nuisance parameters, and (ii) a $N_\ell N_z(2N_z+1) \times N_\ell N_z(2N_z+1)$ covariance matrix Σ. A systematic error may be included as either a nuisance parameter (possibly with a prior), or as an additional contribution to Σ. Here shear calibration and photo-z biases are included as nuisance parameters, and other errors (galaxy biasing and intrinsic alignments) are included in Σ.

c. Power spectrum model

In order to estimate the angular galaxy and convergence power spectra, we need the 3-dimensional power spectrum matrix of the matter m, galaxies g, and convergence reconstructed from intrinsic ellipticity e:[8]

$$\mathbf{P}(k,z) = \begin{pmatrix} P_{mm} & P_{gm} & P_{em} \\ P_{gm} & P_{gg} & P_{ge} \\ P_{em} & P_{ge} & P_{ee} \end{pmatrix}. \tag{A3}$$

(For clarity, we suppress k, z indices where not needed.) This matrix is symmetric because rotational invariance allows one to transform $\mathbf{k} \to -\mathbf{k}$, and in general contains 6 power spectra. We include shot noise in P_{gg} but not P_{ee}.[9]

All 6 of these spectra need to be modeled, but only the matter power spectrum $P_{mm}(k,z)$ is known accurately from theory. We use the Eisenstein and Hu transfer function [52] and the Smith et al. nonlinear mapping [53]. Unlike DETF, we take into account the full $\Omega_{\rm m}$ dependence of the nonlinear mapping for consistency, although its validity for arbitrary $w(z)$ still needs to be studied.

The galaxy spectra are controlled by a bias b_g and stochasticity r_g: $P_{gg} = b_g^2 P_{mm}$ and $P_{gm} = b_g r_g P_{mm}$. Both of these can in general depend on scale and redshift. Similarly for the intrinsic ellipticity, one may define $P_{ee} = b_\kappa^2 P_{mm}$ and $P_{me} = b_\kappa r_\kappa P_{mm}$. This leaves the P_{ge} spectrum undetermined; no specific model is required since we marginalize over it. The fiducial model contains no intrinsic alignments, i.e., $P_{ee} = P_{ge} = P_{me} = 0$.

---

[8] In general e depends on galaxy shapes and hence on the line of sight along which the galaxies are observed; since we will use the Limber approximation one should assume that this line of sight is perpendicular to $\mathbf{k}$.

[9] This is so that we may use the stochasticity r_g as an estimate of how well the galaxy density can be used to trace the mass, but also set $P_{ee} = 0$ in our fiducial model.

The convergence power spectra are given by the standard Limber equation:

$$\begin{aligned} C^{\kappa\kappa}_{\ell ij} &= \frac{9}{16}(\Omega_{\rm m}H_0^2)^2(1+f_i)(1+f_j)\int (1+z)^2 A_i(z)A_j(z)P_{mm}(k,z)\frac{dz}{H(z)} \\ &+\delta_{ij}P_{ee}(k_{(i)},z_i)\frac{H(z_i)}{\Delta z_i} \\ &+\frac{3}{4}\Omega_{\rm m}H_0^2(1+f_j)\frac{A_j(z_i)}{[r(z_i)]^2}P_{em}(k_{(i)},z_i)+(i\leftrightarrow j) \\ &+\frac{\gamma^2_{\rm rms}}{n_i}\delta_{ij}. \end{aligned} \tag{A4}$$

In this equation, the first line represents the pure lensing part of the power spectrum, the second line represents II contamination, the third GI contamination, and the fourth shot noise. We define $k = \ell/r(z)$ where $r(z)$ is the comoving angular diameter distance, n_i the source density in the ith bin, and the lensing strengths are defined by

$$A_i(z) = 2\frac{r(z_i,z)r(z)}{r(z_i)}\Theta(z_i - z), \tag{A5}$$

where $r(z_i, z)$ is the comoving angular diameter distance from the lens redshift z to the source redshift z_i (i.e., the redshift of the galaxies in the ith redshift bin). Θ represents the Heaviside step function.

The parameters f_i in Eq. (A4) are the shear calibration parameters. They are zero for perfect shear estimation; in reality one will have to apply a prior with mean zero and some uncertainty $\sigma(f_i)$. Note that χ, k, and A contain implicit cosmology dependence.

Similarly, the galaxy power spectra are given by

$$C^{gg}_{\ell ij} = \delta_{ij}P_{gg}(k_{(i)},z_i)\frac{H(z_i)}{\Delta z_i}, \tag{A6}$$

where $k_{(i)} = \ell/r(z_i)$ and Δz_i is the width of the ith bin. The galaxy power spectra are not actually used to probe cosmological parameters, however the power spectra are needed in order to construct Σ. The galaxy-convergence spectra are

$$C^{g\kappa}_{\ell ij} = \frac{3}{4}\Omega_{\rm m}H_0^2(1+f_j)\frac{A_j(z_i)}{[r(z_i)]^2}P_{gm}(k_{(i)},z_i) + \delta_{ij}P_{ge}(k_{(i)},z_i)\frac{H(z_i)}{\Delta z_i}, \tag{A7}$$

which is zero for $j < i$ and measures intrinsic alignments for $j = i$.

The shell redshifts z_i are assigned fiducial values so that equal numbers of source galaxies are in each bin, and priors $\sigma(z_i)$ are assigned on the knowledge of the photo-z bias.

d. Covariance matrix model

In the case of Gaussian density and convergence fields, the covariance matrix takes the form of Wick's theorem:

$$\Sigma[C^{AB}_{\ell ij}, C^{A'B'}_{\ell' i' j'}] = \frac{1}{2f_{\rm sky}\ell^2\Delta\ln\ell}\left(C^{AA'}_{ii'}C^{BB'}_{jj'} + C^{AB'}_{ij'}C^{BA'}_{ji'}\right)\delta_{\ell\ell'}, \tag{A8}$$

where A and B represent either g or κ, and the denominator in the prefactor counts the number of modes in a bin.

We include observables for $\ell < 10^4$, but include the non-Gaussian covariances due to the 1-halo term[10] in the matter 4-point function, which has been shown to dominate the excess covariance of the power spectrum on small scales [54]. The galaxy ($gggg$) and galaxy-matter ($ggmm$) trispectra are more complicated to model and not yet included; while we expect that trispectrum effects will be less important for the cross-correlation cosmography ratio tests where one

[10] We do not yet include the dispersion in the concentration-mass relation, which may be significant at the 4-point level [54]. Neither do we include halo triaxiality (which boosts the dispersion in projected concentrations).

does not use the amplitude of the galaxy-matter correlation, this issue deserves future study. The specific equation for this 4-point contribution is

$$\Sigma[C^{\kappa\kappa}_{\ell ij}, C^{\kappa\kappa}_{\ell' i' j'}] \ += \ \frac{81}{256\pi^2 f_{\rm sky}}(\Omega_{\rm m}H_0^2)^4 \int dz\,(1+z)^4 \int dM\,\frac{M^4}{[r(z)]^8} \times \frac{dN}{dz\,dM}[u(k,z,M)u(k',z,M)]^2 \times A_i(z)A_j(z)A_{i'}(z)A_{j'}(z), \tag{A9}$$

where "+ =" means the adding of the right-hand side to the specified covariance matrix element. Here $dN/dz\,dM$ is the number of halos in the whole sky per unit redshift z per unit mass M, and u is the Fourier transform of the halo profile at comoving wavenumber $k = \ell/r(z)$ or $k' = \ell'/r(z)$, normalized to $u(k=0) = 1$. We use the Sheth & Tormen [55] mass function and an NFW [56] mass profile. The concentration-mass relation was taken from the appendix of Voit et al. [57], rescaled to the Sheth & Tormen definition of virial overdensity.

We next marginalize out the galaxy biasing and intrinsic alignment parameters. There are five of these. The galaxy power spectra P_{gg} are easy to marginalize out: one removes all information about $C^{gg}_{\ell ij}$:

$$\Sigma[C^{gg}_{\ell ij}, C^{gg}_{\ell ij}] += \mu, \tag{A10}$$

where $\mu \to \infty$ for all ℓ, i, j.[11]

Any remaining nuisance parameter X associated with the galaxy biasing or intrinsic alignments is taken out by setting:

$$\Sigma[C^{AB}_{\ell ij}, C^{A'B'}_{\ell' i' j'}] += \sigma^2_{\rm prior}(X)\frac{\partial C^{AB}_{\ell ij}}{\partial X}\frac{\partial C^{A'B'}_{\ell' i' j'}}{\partial X}, \tag{A11}$$

where $\sigma^2_{\rm prior}(X)$ is the prior placed on parameter X. We marginalize over $P_{gm}(k,z)$ in each of our ℓ and z-bins (i.e., $N_\ell N_z$ parameters total) with sufficiently large priors that the priors have no effect on the result. (They cannot be infinite for numerical reasons.) This nonparametric marginalization prevents our Fisher matrix from taking advantage of any functional form we specify. A similar method is used for $P_{ee}(k,z)$ (which effectively removes shear auto-powers within the same bin) and $P_{ge}(k,z)$. For $P_{me}(k,z)$, which has the most significant degrading effect on cosmological parameters, we implement a prior in each bin to prevent unrealistically large intrinsic alignments. This prior is described and justified in §A 2 h.

e. Shear calibration errors

Shear calibration errors are multiplicative errors on the shear γ: $\gamma \to (1+f)\gamma$. The calibration error f must be taken to depend on redshift z because as a function of redshift one observes galaxies of different types (morphology, radial profile) and colors (hence different PSF!). The STEP simulations [58] have shown that in simulations with a wavelength (λ)-independent PSF, several shape measurement methods currently achieve shear calibration better than 2% ($|f| < 0.02$). With further STEP-like exercises with simulated galaxies that closely resemble the observed morphologies of the actual DES sample, we anticipate further reductions in $|f|$. In the near future, the shear calibration may become limited by λ-dependent PSF effects: galaxies whose light is dominated by longer wavelengths with smaller PSFs will have larger calibration than galaxies dominated by short wavelengths. The lensing community is in the early stages of thinking about this problem, so we have not assumed that advanced solutions[12] will be available for pre-JDEM.

We noted that for a ground-based system with seeing limited by Kolmogorov-spectrum turbulence in the atmosphere, the PSF 2nd moments scale as $\lambda^{-2/5}$. For a galaxy with typical resolution factor of about 0.5 (as defined in Hirata & Seljak [59]) the shear calibration changes by 0.4% for every 1% change in effective wavelength. The RMS fluctuation in wavelength for the extreme case of an emission line sitting in a filter of width $\Delta\lambda/\lambda = 0.25$ is $0.25/\sqrt{12} = 0.072$,

---

[11] Technically the $i \neq j$ galaxy cross-powers need not be marginalized out because they should be zero in the fiducial model; however we assume that they will be used to constrain photo-z outlier models and hence should not be used again in the determination of cosmological parameters.

[12] This would include, for example, decomposing multicolor galaxy images into star-forming and old stellar population components, convolving with model SEDs for each component and fitting a shape.

corresponding to a shear calibration fluctuation of 0.029. A single emission line causes the worst damage, but most galaxies in most filters have only a small fraction of their emission in lines. As a first estimate of the more realistic case, we took 20% of the single-line case, assigning a shear calibration error of 0.0058.[13] We take one bin ($\Delta \ln a \sim 0.1$) as a reasonable correlation length for the shear calibration systematic because a galaxy redshifts through a filter in $\Delta \ln a \sim 0.25$. A systematic that depends on e.g., an emission line appearing in the red or blue side of a filter should change sign twice during a filter passage. Therefore a prior of $\sigma(f_i) = 0.0058$ was applied independently in each z-bin.

f. Photometric redshifts

We assume that in about 2015 there will be available an *unbiased* spectroscopic redshift survey of order 10^5 galaxies down to the DES limit of $I_{\rm AB} \approx 23.5$ mag. With this size spectroscopic survey, the ability to constrain the photo-z error properties will be dominated by two systematic errors: (i) incompleteness due to redshift failures, and (ii) photometric calibration or extinction fluctuations in the lensing survey (such that the spectroscopically targeted regions are not representative of the whole). These cannot be fully assessed with the information available and without knowing the extent of the resources that will be brought to bear on the photo-z problem. A simple calculation shows that losing 5% of the galaxies, all on one tail of the distribution, would lead to a bias of $0.005(1+z)$ in the resulting photo-z error distribution. A bias of the same order of magnitude might be expected to arise from about a 1% photometric calibration fluctuations (suppressed by a factor of a few due to the spectroscopic survey covering several patches in the larger WL survey area).

The "nightmare" scenario is the existence of a class of photo-z outliers with no features strong enough to identify a spectroscopic redshift. While cross-correlation techniques [60] should be able to identify this problem, one is left with the ambiguity in the bias of the outliers since angular correlations only measure the product of bias and redshift distribution $b\,dN/dz$ [39] (with corrections due to stochasticity on nonlinear scales). We have assumed that the combination of spectroscopic surveys and galaxy correlations can constrain the photo-z bias to a 1σ error of $0.005(1+z)$, but this number is in urgent need of refinement.

g. Galaxy biasing and cross-correlation cosmography

In WL surveys, there is potentially much to gain in using the galaxy density as an indicator of the underlying mass distribution. An example is the use of the source redshift dependence of galaxy-shear correlations in lensing cross-correlation cosmography [61, 62]. This is true even if the bias b_g and stochasticity r_g of the galaxy density are poorly known. The gain from this approach depends on the correlation coefficient of galaxy density r_g with respect to mass. We assume a fiducial model in which $r_g = 0.9$ in the linear regime, dropping to $r_g = 0.6$ in the non-linear regime.

Galaxy density information is completely rejected by marginalizing over b_g and r_g in each of the 10 redshift bins and 18 angular-scale bins. Note that this procedure preserves information in the lensing distance ratio test.

h. Intrinsic alignments

We take a fiducial model with no intrinsic alignments, so that it is impossible for intrinsic alignments to be used to predict the local mass distribution. If b_κ is large and the IA model is sufficiently restrictive, it is possible for the Fisher matrix to take advantage of the cosmology dependence of the intrinsic alignments, which is an undesired result [63].

Intrinsic alignment models must be allowed to be functions of redshift and of angular scale in a realistic forecast. GI and II effects are treated separately. GI depends on the matter-IA correlation ($b_\kappa r_\kappa$) whereas II depends on b_κ^2. We completely marginalize over II, i.e., we allowed b_κ^2 to float independently in each (z, ℓ) bin. This is equivalent to rejecting the shear power spectra within a z-slice and only taking cross-spectra [64]; this may be conservative but little information is lost through complete marginalization over II. In the case of GI, we assumed that in the linear regime (crudely modeled as $\ell < 300$) galaxies trace the matter well enough that the galaxy-intrinsic ellipticity correlation

[13] The effective wavelength of the PSF can also be affected by breaks in the spectrum. For a galaxy with a factor of 2 break in the SED in the center of the bandpass, the effective wavelength is shifted by 2% from a flat SED, corresponding to a shear calibration fluctuation of 0.008.

could be used to infer the matter-intrinsic alignment correlation $b_\kappa r_\kappa$ and apply the corresponding small correction to the lensing data (expected to be around 3σ according to the Hirata et al. IA model B [65]). On nonlinear scales, we applied a weak prior on $b_\kappa r_\kappa$ to prevent it from being much larger than the observed IA signal of $|b_\kappa r_\kappa| \sim 0.003$ [66]. In the absence of knowledge of the "correct" form for such a prior, we used

$$\sigma(b_\kappa r_\kappa) = 0.003\sqrt{N_{\ell,\rm nonlin}(N_z - 1)}, \tag{A12}$$

applied independently in each (z, ℓ) bin in the nonlinear regime. This choice was motivated by requiring that we not be able to constrain $b_\kappa r_\kappa$ to better than 0.003 by "averaging down" the prior in the different (z, ℓ) bins. We use $N_z - 1$ instead of N_z in the above formula because $b_\kappa r_\kappa$ in the highest-z bin has no effect on the observed power spectra.

The 0.003 number is highly uncertain as it results from an extrapolation of SDSS data to moderate redshift. It will have to be revisited after either SDSS spectroscopic intrinsic alignment analyses [65] can be repeated on higher-redshift samples, or photometric WL surveys such as DES provide a refined estimate of the order of magnitude of $b_\kappa r_\kappa$. A particularly nasty (but possible) scenario would be that galaxy alignments are strong during the peak era of galaxy formation at $z > 1$, but decay at later times as galactic disks precess and de-align in their dark matter halos. In this case the intrinsic alignment signal even at $z \sim 0.6$ could be much stronger than in SDSS and we may be forced to the pessimistic option of completely marginalizing over $b_\kappa r_\kappa$ in the nonlinear regime.

3. Pre-JDEM Baryon Acoustic Oscillation Fisher Matrix

Forecasts for the baryon acoustic oscillations were computed using the formulae from Seo and Eisenstein [67]. This produces fractional errors on $D_A(z)/s$ and $H(z)s$, where s is the sound horizon and varies with $\Omega_m h^2$ and $\Omega_b h^2$. In all cases, the errors on D_A/s and Hs are mildly covariant, with a coefficient of 0.4 (in the sense that a larger D_A tends to have a larger H).

We used redshift bins identical to the $w(z)$ parametrization. Each bin was said to yield an independent constraint on the distance scale. The comoving volume in each bin was used to scale the answer from the large volume limit; i.e., no boundary effects were considered. This should be a reasonable approximation for large surveys and slow variations in $w(z)$. Note that although $w(z)$ was given a very flexible parametrization, the cosmological constraints are such that only slow variations are well measured.

For simplicity, each survey was taken to have a constant comoving number density n and a constant amplitude of the power spectrum $P_{0.2}$. This is not exact but it is hard to see how it could alter the results at any level that would affect a JDEM choice. For convenience, we registered the redshift range of the surveys to the redshift binning. The power spectrum was taken to be anisotropic according to the linear Kaiser model, with β computed from $f = \Omega_m^{0.6}(z)$ and the bias.

It should be noted that these are not exact models of the surveys, but they do capture the scope and redshift range of the projects.

No systematic errors were included. Simulations show no evidence for systematic errors in the acoustic scale at the level of precision of these surveys, nor are survey selection effects expected to pose any insurmountable problems [68, 69].

The degradation of the acoustic scale due to non-linear structure formation was included assuming that $\Sigma_\perp = 9(D/D_0)h^{-1}$ Mpc, where D is the growth function and D_0 is that function at $z = 0$. The transverse degradation was $\Sigma_\parallel = \Sigma_\perp(1 + f)$.

Density-field reconstruction was included as a multiplicative reduction in these two non-linear parameters. The best-case multipliers were taken to be 0.5, but some sparser samples were given 75% or even 100% of the non-linearity.

The surveys employed are listed in Table II.

We omitted the high-redshift WFMOS data set arbitrarily as we were including BOSS and HETDEX at high redshift. Including any two of the three planned experiments gives similar results.

These distance estimates include only the results from the BAO scale. It is likely that these redshift surveys will yield other cosmological information relevant to dark energy, e.g., the redshift distortion and Alcock-Paczynski methods described in Sec. IV A 4. Both require detailed modeling of non-linear structure formation and galaxy clustering bias. If this modeling can be done accurately, the dark energy information could be substantially improved, and this promise is driving considerable research on these topics.

Survey	Redshift[a]	Area	σ_8	# of galaxies	Non-linearity
WiggleZ	$0.6 < z < 1.0$	1000 deg^2	0.8	0.4M	75%
BOSS	$0.08 < z < 0.48$	10,000 deg^2	1.5	0.8M	50%
BOSS	$0.48 < z < 0.67$	10,000 deg^2	1.5	0.4M	50%
BOSS Ly-α	$2.08 < z < 2.64$	8000 deg^2	0.25	7.5M[b]	100%
WFMOS	$0.60 < z < 1.0$	2000 deg^2	0.8	2M	50%
WFMOS	$1.00 < z < 1.35$	2000 deg^2	0.8	1.5M	50%
HETDEX	$1.86 < z < 3.44$	420 deg^2	0.8	0.8M	50%
Photo-z surveys[c]	$0.67 < z < 1.10$	20,000 deg^2	1.4	10M	100%

[a]Redshift ranges picked to match the bin boundaries in $w(z)$, hence the non-standard values.
[b]Number of "galaxies" picked to give aggregate D error of 1.7% and H error of 1.5%, so as to match the BOSS Lyman α forest forecast.
[c]4% fractional error in $1 + z$

TABLE II: A description of the BAO surveys assumed in the FoMSWG pre-JDEM data model.

4. Pre-JDEM Supernova Fisher Matrix

a. The Importance of Systematic Uncertainties

The best-established method for measuring the history of cosmic expansion is the use of luminosity distances to supernovae (Type Ia). Our goal here is to estimate the sample of supernova observations that will be available at the time of a JDEM launch, taken to be 2016, so that we can measure the incremental impact of a JDEM on knowledge of cosmological parameters using our figure-of-merit. Our conclusion detailed below, is that making reasonable assumptions about observing programs that have, and have not yet been carried out, the samples at all redshifts below 0.8 will be large enough to make statistical errors irrelevant, provided there is no stringent reduction of the usable number of objects by selecting for a narrow set of host galaxy or supernova properties. This means that systematic errors, that are not reduced by increasing the sample size, will dominate. Such systematic errors are difficult to enumerate and measure. The only certain way to see their effect is to compare independent results from completely different techniques. The task ahead for supernova cosmology is to explore the best ways to measure and, if possible, reduce these distance errors. The task for a JDEM proposer will be to describe their program for improving on what will have been done by 2016 in the statistical language of the FoMSWG. We caution that making less realistic assumptions about systematic errors is the simplest way to show "improvement" in the figure of merit. If used in this way, the figure of merit could reward the least realistic and punish the most thoughtful proposal.

What are the systematic errors that keep today's distance measurements from achieving the precision set by statistical error? There are many. These include photometric calibration across a factor of 10 in wavelength from the U-band to the near infrared, and a factor of 10^6 in flux from the nearest supernovae (in the Hubble flow) to the most distant objects detected by HST. They include peculiar velocities and regional flows that may affect the correct interpretation of the velocity-distance relation. They include uncorrected selection effects and genuine evolution in the mean properties of the nearby and distant samples.

But most importantly, they include errors that result from the way in which the light curves are used to infer the distances. The rise and decline of SN Ia light curves are closely linked to the intrinsic luminosity of the supernova: measuring the shape of the light curve allows the uncertainty in distance for a single supernova to be reduced from roughly 50% to under 10%. An additional source of uncertainty comes from the effects of interstellar dust, both in our Galaxy and in the supernova host. Interstellar dust does not absorb equally at all wavelengths. The current evidence from supernovae [70] shows that the ratio of total absorption to absorption at a particular color that gives the smallest dispersion in supernova results is not the value usually associated with dust in our Galaxy. The net result is that inferences about cosmological parameters (such as w) are systematically different depending on which light curve fitter is used, and which method of accounting for the effect of dust is employed. Estimates of the magnitude of these effects vary, and are generally in the range of 7-10%, but there is currently no published result where the systematic effect on w is claimed to be smaller than 6% . External validation of systematic uncertainty estimates would demand independent sets of low- and high-redshift data and a comparison of the results obtained with a variety of approaches to light curve fitting and extinction corrections.

One path to avoiding the systematics of dust and evolution is to discard a large fraction of the discoveries, while retaining only those in elliptical galaxies. This requires a careful demonstration that the supernovae in ellipticals can give a better cosmological result and confidence that the dust absorption in ellipticals is fully understood.

A possible path to better understanding of the dust that obscures and reddens supernovae may come from observations made in the rest-frame near infrared (J,H,K bands). Preliminary indications are that SN Ia are more similar to one another at infrared wavelengths than in the optical bands, and the effects of dust are smaller by about a factor of 3 [71]. The combined analysis of optical and infrared data has the potential to determine the dust properties for individual objects [72] and to place this subject on firmer footing.

In summary, we are reluctant to assume that these unsolved systematic problems in supernova cosmology will evaporate in the next 7 years (before JDEM). Therefore, we assume a conservative floor to the distance uncertainties, amounting to 2% in distance in each bin of width $\Delta z = 0.1$ for $z \leq 0.5$, and 3% in distance in each bin of width $\Delta z = 0.1$ for $z \geq 0.5$. The systematic distance errors are taken to be statistically independent from bin to bin. The discussion below will show that present and future SN surveys are likely to detect enough SNe to reduce statistical distance errors below these systematic floors for all $z < 0.9$.

In the computation of the FoMSWG figure of merit example for the most significant principal components, the assumed JDEM sample was that used by the DETF.

b. Assumptions about pre-JDEM SNe Surveys

The early results of the High-Z Team [73] and the Supernova Cosmology Project [74] provided clear evidence for cosmic acceleration, and, because they used different approaches for using the light curve shape to determine the absolute magnitude, as well as different samples of high redshift supernova, provided some external tests of the estimated errors. The DETF made some forecasts of the available data for Stage II and Stage III supernova samples. Since then, the samples at high redshift ($z \sim 0.5$) have been substantially augmented, especially by the ESSENCE program [75], the Supernova Legacy Survey [76] and at $z > 1$, in a development not considered by the DETF, by the Higher-Z program on HST [77, 78]. The published samples at low redshift, which are equally important in deriving the cosmology, have also been augmented by SN Ia light curves from the CfA [79] and the SCP [80]. Another important development, not anticipated by the DETF, has been the SDSS Supernova Survey, which has good light curves (better than 5 epochs, with one before maximum) and spectra for confirming the supernova type and determining its redshift for 300 objects in the redshift range $0.1 < z < 0.3$.

redshift bin	number of SNIa
< 0.1	500
0.1-0.2	200
0.2-0.3	320
0.3-0.4	445
0.4-0.5	580
0.5-0.6	660
0.6-0.7	700
0.7-0.8	670
0.8-0.9	110
0.9-1.0	80
1.0-1.1	25
1.1-1.2	16
1.2-1.3	16
1.3-1.4	4
1.4-1.5	4
1.5-1.6	4
> 1.6	4

TABLE III: The number of SNIa in various redshift bins assumed in constructing the pre-JDEM data model.

Looking ahead, we note that the low-redshift sample is on the verge of rapid expansion. In the past year, the SCP added 8 objects to the low-z data set [80]. The CfA SN program has 150 more, most of which will pass the same data cuts, the Carnegie SN program promises 200 light curves, and the KAIT program at the Lick Observatory has approximately 150 to contribute. While there may be some overlap among these objects, the DETF assumption of 500 well-observed nearby objects seems reasonable. Skymapper, a survey telescope in Australia, will create a well-sampled and carefully controlled set of 150 low-z supernovae, once it begins operation in 2009. At redshifts above 0.1, there

	z_p	$\sigma(w_p)$	$\sigma(w_a)$	$\sigma(\Delta\gamma)$
SNe+Planck	0.01	0.34	6.97	—
WL+Planck	0.50	0.09	1.20	0.51
SN+WL+Planck	0.36	0.05	0.68	0.39
BAO+Planck	0.52	0.04	0.44	—
All	0.49	0.03	0.31	0.21

TABLE IV: Pre-JDEM expansion and growth history parameter errors. For each combination of probes, we show the redshift pivot values z_p, 68% C.L. Fisher matrix errors on the DETF parameters w_p and w_a, and the growth index γ. We have projected parameters describing the equation of state $w(z)$ onto the (w_p, w_a) subspace and, to report these errors, fixed the parameters γ and $\ln G_0$ while marginalizing over the other six parameters. The error on γ, on the other hand, assumes marginalization over all other 44 parameters.

will be no extension of the SDSS Supernova Survey and no continuation of the Supernova Legacy Survey. However, there will be the advent of a supernova survey that follows up the "medium-deep" fields of Pan-STARRS. This should begin in 2009. We assume it will run for 40 months, although this is not yet guaranteed. We were provided a table of the expected number of supernova light curves in each redshift bin per month, and have incorporated a total of 500 objects into our pre-JDEM priors. We also assume that the HST servicing mission will achieve its goals, and that HST will be used in the next 5 years to provide a sample of supernovae beyond $z = 1$ that is 4 times as large as the present published sample. The Dark Energy Survey is an ambitious plan to build a large-format camera for the 4-meter Blanco telescope at CTIO. We thank the DES SN working group for providing us with their current projections of DES performance in advance of a final determination of the DES strategy. Adding their projected sample of 3000 objects, but truncating the sample beyond redshift of 0.8 (which is a conservative assumption), we construct the following table, which we believe represents a reasonable estimate of what will be available for detailed cosmological analysis in 2016 (the beginning of the JDEM mission).

Current methods for estimating distances to individual objects have an uncertainty that is reckoned to be below 10%, so even accounting for photometric uncertainty, the sample sizes out to a redshift of 0.8 will be sufficiently large that the present systematic floor will be the dominant uncertainty in each redshift bin. As we emphasized above, this estimate is difficult to verify, and limits the precision that is reasonable to ascribe to a Figure of Merit. While most of the supernovae in this table come from DES, we note that the sample size predicted for the Pan-STARRS program would be sufficient to make the systematic floor into the effective limit on the distance measurement at these redshifts. The supernovae beyond redshift 1 will be extremely interesting, but their statistics will not be sufficient to bring them down to the systematic floor. For these objects, an independent distance error of 30% per object has been assigned.

APPENDIX B: PRE-JDEM PERFORMANCE

After constructing the Fisher matrices as described in Appendix A, we followed the procedure outlined in Sec. V. The results are summarized in Table IV.

The FoMSWG Fisher matrices for individual techniques, as well as the techniques in combination, can be found on the FoMSWG website `http://jdem.gsfc.nasa.gov/FoMSWG`. Brief explanations of the format of the Fisher matrices (which follows the format defined here) can be found there.

Also at the above website is a `C` program to take the pre-JDEM Fisher matrices as input and combine them in various ways to produce output files of the principal components, the uncertainties in the coefficients of the principal components, information about the DETF $\sigma(w_0)$ and $\sigma(w_a)$, and other information. There is also the option of including additional Fisher matrices (say for an imagined JDEM or for a different realization of a pre-JDEM Fisher matrix). A guide to the software tools is described in the next section.

1. Practical Guide to the FoMSWG Software

In association with this publication, we provide some basic software to help perform the analyses outlined herein. The software package is available from the JDEM website as a gzipped tarball (named `public_fomswg_code.tar.gz`) and contains the following items in the main directory `/PUBLIC_CODE`:

- `fisher_fomswg.c`, which is the main C program for computing the Principal Components and their accuracies. This uses standard C libraries.
- `nrutil.c`, which provides some Numerical Recipes [81] utilities adapted for double precision.
- `function.c`, which contains specific functions for the manipulation of matrices.
- The `/DATA` sub-directory which contains the matrices discussed in Sec. III B for Planck and the pre–JDEM BAO, SN and WL observations (see Appendix A for a detailed explanation of the assumptions that when into constructing these matrices). Note that some matrices have maximal indices less than 44 or are missing a few lower indices; this is simply due to the fact that the technique is insensitive to the parameter in question (as listed in Sec. III B). The associated Fisher matrix elements will thus be zero (explicitly listing these elements as zeros in data-files is equivalent and also works).
- A compiled executable, `fish`, is provided and may work immediately on a linux-based system. If not, a `makefile` is provided which should allow the code to be compiled on most UNIX/Linux systems (we have compiled the code under Mac OSX, Debian, SuSE and IRIX). To compile the code, remove the old `fish` executable and create a new one by typing `make fish`.

The `fish` program can be run from the command line using the default matrices given in the `/DATA` sub-directory, or the user can input a customized matrix (as long as it follows our conventions). To study multiple techniques of the user's choosing, the user should add the respective Fisher matrices and input only the single, combined matrix.

In default mode, the user can select from eight possible combinations of SN, BAO, WL, and Planck, and the `fish` program provides a variety of numerical outputs, which are stored in the `/OUTPUTS` sub-directory and displayed on screen.

The screen outputs include:

- Errors on the parameters w_0 and w_a, marginalized over all other 9 parameters.
- DETF FoM (defined as $[\sigma(w_a) \times \sigma(w_p)]^{-1}$).
- Pivot redshift (z_p) and the uncertainty in the associated pivot equation of state (w_p), see Eq. (26).
- Error in constant w, marginalized over all other 9 parameters.
- The growth index, γ, and its FoM [defined as $\sigma^{-2}(\Delta\gamma)$] if the user selects options including WL measurements (options 2, 4, 5, 8).

If the user picks options (1, 3, 6, 7) that only include combinations of SN, BAO and Planck (i.e., geometrical measurements), then γ and G_0 are fixed and the following file outputs are provided:

- `sigma.dat`, which contains the errors on the 36 Principal Components (with and without priors).
- `PC_1234.dat`, which contains the first four eigenvectors.
- `PC_all.dat`, which contains all 36 eigenvectors. Both are provided as a function of redshift (36 bins) as discussed in Sec. III A.
- `w0wa.dat`, which is a 2×2 Fisher matrix for the w_0 and w_a parameterization.

For other options, which include the WL measurements (options 2, 4, 5, 8), the program provides an extra set of files (in addition to the ones listed above) which allow γ (and G_0) to vary. These files have the same naming scheme as above, but with an additional `_gamma` phrase attached, e.g., `sigma_gamma.dat`.

The software is provided to help people become accustomed with the analyses outlined herein, but has not been rigorously tested, and the user is urged not to use its outputs blindly without checking them. Comments on the code should be sent to Dragan Huterer, who deserves the credit for producing this tool.

---

[1] Two recent reviews of dark energy are E. J. Copeland, M. Sami and S. Tsujikawa, Int. J. Mod. Phys. D **15**, 1753 (2006), and J. A. Frieman, M. S. Turner, and D. Huterer, Ann. Rev Astron. and Astrop. **46**, 385 (2008).
[2] See, e.g., G. J. Toomer, *Ptolemy's Almagest* (Princeton University Press, 1998).
[3] R. Bousso and J. Polchinski, JHEP **0006**, 006 (2000),
[4] S. Kachru, R. Kallosh, A. Linde and S. P. Trivedi, Phys. Rev. D **68**, 046005 (2003).
[5] R. Bousso, Gen. Rel. Grav. **40**, 607 (2008).
[6] L. Dyson, M. Kleban and L. Susskind, JHEP **0210**, 011 (2002)
[7] A. Albrecht and L. Sorbo, Phys. Rev. D **70**, 063528 (2004)
[8] G. Efstathiou, W. J. Sutherland and S. J. Maddox, Nature **348**, 705 (1990).
[9] M. Barnard, A. Abrahamse, A. Albrecht, B. Bozek and M. Yashar, Phys. Rev. D **78**, 043528 (2008)
[10] For a review, see L. Amendola, R. Gannouji, D. Polarski and S. Tsujikawa, Phys. Rev. D **75**, 083504 (2007).
[11] For a braneworld review, see R. Maartens, Living Rev. Rel. **7**, 7 (2004). There are many braneworld modifications that are possible explanations of dark energy, or at least modify gravity. For example, see, P. Binetruy, C. Deffayet, U. Ellwanger and D. Langlois, Phys. Lett. **B 477**, 285 (2000); C. Deffayet, G. R. Dvali and G. Gabadadze, Phys. Rev. D **65**, 044023 (2002); R. Gregory, V. A. Rubakov and S. M. Sibiryakov, Phys. Lett. **B 489**, 203 (2000); G. R. Dvali, G. Gabadadze and M. Porrati, Phys. Lett. **B 485**, 208 (2000); C. Csaki, J. Erlich, T. J. Hollowood and J. Terning, Phys. Rev. D **63**, 065019 (2001); I. I. Kogan, S. Mouslopoulos, A. Papazoglou, G. G. Ross and J. Santiago, Nucl. Phys. **B 584**, 313 (2000).
[12] A. Albrecht *et al.*, *Report of the Dark Energy Task Force,* arXiv:astro-ph/0609591.
[13] D. J. Eisenstein, H. Seo, E. Sirko, and D. N. Spergel, Astrophys. J. **664** 675 (2007).
[14] P. Rosati, S. Borgani, and A. Norman, Ann. Rev Astron. and Astrop. **40**, 539 (2002).
[15] E. S. Rykoff *et al.*, Mon. Not. Roy. Astron. Soc. **387**, L28 (2008).
[16] G. W. Pratt, J. H. Croston, M. Arnaud and H. Boehringer, *Galaxy cluster X-ray luminosity scaling relations from a representative local sample (REXCESS),* arXiv:0809.3784 [astro-ph].
[17] A. V. Kravtsov, A. Vikhlinin, and D. Nagai, Astrophys. J. **650**, 1 (2006).
[18] M. Arnaud, E. Pointecouteau and G. W. Pratt, Astronomy and Astrophysics **474**, L37 (2007).
[19] J. D. Cohn, A. E. Evrard, M. White, D. Croton and E. Ellingson, Mon. Not. Roy. Astron. Soc. **382**, 1738 (2007).
[20] S. Majumdar and J. J. Mohr, Astrophys. J. **613**, 41 (2004).
[21] M. Lima and W. Hu, Phys. Rev. D **70**, 043504 (2004); Phys. Rev. D **72**, 043006 (2005).
[22] P. Schuecker *et al.*, Astron and Astrop. **398**, 867 (2003).
[23] S. W. Allen *et al.*, Mon. Not. Roy. Astron. Soc. **383**, 879 (2008).
[24] A. Vikhlinin *et al.*, *Chandra Cluster Cosmology Project II: Samples and X-ray Data Reduction,* arXiv:0805.2207 [astro-ph].
[25] D. E. Johnston *et al.* [SDSS Collaboration], *Cross-correlation Weak Lensing of SDSS galaxy Clusters II: Cluster Density Profiles and the Mass–Richness Relation,* arXiv:0709.1159 [astro-ph].
[26] L. Guzzo *et al.*, Nature **451**, 541 (2008).
[27] N. Kaiser, Mon. Not. Roy. Astron. Soc. **227**, 1 (1987).
[28] Y. Wang, JCAP **05**, 021 (2008).
[29] E. Linder, Astropart. Phys. **29**, 336 (2008).
[30] A. J. Hamilton, in *The Evolving Universe,* ed. D. Hamilton, (Kluwer, p. 185, 1998).
[31] V. Aquaviva, A. Hajian, D. Dn. Spergel, S. Das, Phys. Rev. D **78**, 043514 (2008).
[32] Y.-S. Song, and W. J. Percival, *Reconstructing the History of Structure Formation using Peculiar Velocities,* arXiv:0807.0810 [astro-ph].
[33] W. Percival and M. White, *Testing cosmological structure formation using redshift-space distortions,* arXiv:0808.0003 [astro-ph].
[34] L. Verde, *et al.,* Mon. Not. Roy. Astron. Soc. **335**, 432 (2002).
[35] P. Mc Donald and U. Seljak, *How to measure redshift-space distortions without sample variance,* arXiv:0810.0323 [astro-ph].
[36] M. White, Y.-S. Song, and W. J. Percival, *Forecasting Cosmological Constraints from Redshift Surveys,* arXiv:0810.1518 [astro-ph].
[37] R. K. Sachs and A. M. Wolfe, Astrophys. J. **147**, 73 (1967).
[38] R. G. Crittenden and N. Turok, Phys. Rev. Lett. **76**, 575 (1996).
[39] S. Ho, C. Hirata, N. Padmanabhan, U. Seljak and N. Bahcall, Phys. Rev. D **78**, 043519 (2008).
[40] T. Giannantonio, R. Scranton, R. G. Crittenden, R. C. Nichol, S. P. Boughn, A. D. Myers and G. T. Richards, Phys. Rev. D **77**, 123520 (2008).
[41] N. Afshordi, Phys. Rev. D **70**, 083536 (2004).
[42] C. Alcock and B. Paczynski, Nature **281**, 358 (1979).
[43] W. E. Ballinger, J. A. Peacock, and A. F. Heavens, Mon. Not. Roy. Astron. Soc. **282**, 877 (1996).
[44] T. Matsubara and A. S. Szalay, Astrophys. J. **556**, L67 (2001).

[45] M. Shoji, D. Joeng, and E. Komatsu, *Extracting Angular Diameter Distance and Expansion Rate of the Universe from Two-dimensional Galaxy Power Spectrum at High Redshifts: Baryon Acoustic Oscillation Fitting versus Full Modeling,* arXiv:0805.4238 [astro-ph].
[46] N. Ross, et al., Mon. Not. Roy. Astron. Soc. **381**, 573 (2007).
[47] D. Huterer and G. Starkman, Phys. Rev. Lett. **90**, 031301 (2003).
[48] E. V. Linder, Phys. Rev. D **72**, 043529 (2005).
[49] The Planck Collaboration, *Planck: The scientific programme,* arXiv:astro-ph/0604069.
[50] L. Page, *et al.*, Astrophys. J. Suppl. **170**, 335 (2007).
[51] G. Holder, Z. Haiman, M. Kaplinghat and L. Knox, Astrophys. J. **595**, 13 (2003).
[52] D. J. Eisenstein, and W. Hu, Astrophys. J. **496** 605 (1998).
[53] R. E. Smith *et al.* [The Virgo Consortium Collaboration], Mon. Not. Roy. Astron. Soc. **341**, 1311 (2003).
[54] A. Cooray and W. Hu, Astrophys. J. **554**, 56 (2001).
[55] R. K. Sheth and G. Tormen, Mon. Not. Roy. Astron. Soc. **308**, 119 (1999).
[56] J. F. Navarro, C. S. Frenk and S. D. M. White, Astrophys. J. **490**, 493 (1997).
[57] G. M. Voigt *et al.*, Astrophys. J. **593**, 272 (2003).
[58] R. Massey *et al.*, Mon. Not. Roy. Astron. Soc. **376**, 13 (2007).
[59] C. M. Hirata and U. Seljak, Mon. Not. Roy. Astron. Soc. **343**, 459 (2003).
[60] J. A. Newman, Astrophys. J. **684**, 88 (2008).
[61] B. Jain and A. Taylor, Phys. Rev. Lett. **91**, 141302 (2003).
[62] G. M. Bernstein and B. Jain, Astrophys. J. **600**, 17 (2004).
[63] S. Bridle and L. King, New J. Phys. **9**, 444 (2007).
[64] M. Takada and M. J. White, Astrophys. J. **601**, L1 (2004).
[65] C. M. Hirata *et al.*, Mon. Not. Roy. Astron. Soc. **381**, 1197 (2007).
[66] C. Heymans *et al.*, Mon. Not. Roy. Astron. Soc. **371**, 750 (2006).
[67] H. Seo and D. J. Eisenstein, Astrophys. J. **633**, 575 (2005).
[68] H. Seo, E. R. Siegel, D. J. Eisenstein, and M. White, Astrophys. J. **686**, 13 (2008).
[69] A. G. Sánchez, C. M. Baugh, and R. Angulo, Mon. Not. Roy. Astron. Soc. **390**, 1470 (2008).
[70] A. Conley *et al.*, Astrophys. J. **664**, L13 (2007).
[71] M. Wood-Vasey *et al.*, *Type Ia Supernovae are Good Standard Candles in the Near Infrared: Evidence from PAIRITEL,* arXiv:0711.2068 [astro-ph].
[72] K. Krisciunas *et al.*, Astron. J. **133**, 58. (2007)
[73] A. Riess *et al.*, Astron. J. bf 116, 1009 (1998).
[74] S. Perlmutter *et al.*, Astrophys. J. **517**, 565 (1999).
[75] M. Wood-Vasey *et al.*, Astrophys. J. **666**, 716 (2007).
[76] Astier, P. *et al.*, Astronomy and Astrophysics **447**, 31 (2006).
[77] A. Riess *et al.*, Astrophys. J. **607**, 665 (2004).
[78] A. Riess *et al.*, Astrophys. J. **659**, 98 (2007).
[79] S. Jha, A. Riess, and R. Kirshner Astrophys. J. **659**, 122 (2007).
[80] M. Kowalski *et al.*, Astrophys. J. **686**, 749 (2008).
[81] W. H. Press, S. A. Teukolsky, W. T. Vetterling, and B. P. Flannery, *Numerical Recipies in C: The Art of Scientific Computing: Second Edition (1992)*, (Cambridge University Press, Cambridge, 1992).